NONLINEAR IDENTIFICATION AND OPTIMAL FEEDFORWARD FRICTION COMPENSATION FOR A MOTION PLATFORM

A THESIS SUBMITTED TO

THE GRADUATE SCHOOL OF ENGINEERING AND SCIENCE

OF BILKENT UNIVERSITY

IN PARTIAL FULFILLMENT OF THE REQUIREMENTS FOR

THE DEGREE OF

MASTER OF SCIENCE

IN

MECHANICAL ENGINEERING

By

Ahmet Furkan Güç

June 2020

NONLINEAR IDENTIFICATION AND OPTIMAL FEEDFORWARD FRICTION COMPENSATION FOR A MOTION PLATFORM

By Ahmet Furkan Güç

June 2020

We certify that we have read this thesis and that in our opinion it is fully adequate, in scope and in quality, as a thesis for the degree of Master of Science.

Onur Özcan(Advisor)

Melih Çakmakcı

İsmail Uyanık

Approved for the Graduate School of Engineering and Science:

Ezhan Karaşan
Director of the Graduate School

ABSTRACT

NONLINEAR IDENTIFICATION AND OPTIMAL FEEDFORWARD FRICTION COMPENSATION FOR A MOTION PLATFORM

Ahmet Furkan Güç
M.S. in Mechanical Engineering
Advisor: Onur Özcan
June 2020

We present a method of nonlinear identification and optimal feedforward friction compensation procedure for an industrial single degree of freedom motion platform. The platform suffers from nonlinear dynamic effects, such as friction and backlash in the driveline, along with precise reference tracking requirements. In order to eliminate the nonlinear dynamic effects and obtain precise reference tracking, we first identified the system using nonparametric identification with Best Linear Approximation (BLA). Next, the feedback controller is implemented as a classical PI controller and it is designed using loop shaping techniques so that the system meets the linear system requirements. Then, we identified the nonlinear dynamics of the platform using Higher Order Sinusoidal Input Describing Function (HOSIDF) based system identification and we present optimal feedforward compensation design to improve reference tracking performance. We modeled the friction characteristics using the Stribeck friction model and identified through a procedure with a special reference signal and the Nelder-Mead algorithm. Results indicate that the RMS trajectory error decreased from 0.0431 deg/s to 0.0117 deg/s, and standart deviation of speed reference error integral decreased from 0.0382 deg to 0.0051 deg, when the proposed nonlinear identification and friction compensation method is used.

Keywords: Feedforward control, Friction compensation, System identification, Nonlinear systems.

ÖZET

BİR HAREKET PLATFORMU İÇİN DOĞRUSAL OLMAYAN TANILAMA VE OPTİMAL İLERİ BESLEME SÜRTÜNME KOMPANZASYONU

Ahmet Furkan Güç
Makine Mühendisliği, Yüksek Lisans
Tez Danışmanı: Onur Özcan
Haziran 2020

Bir serbestlik derecesine sahip endüstriyel hareket platformu için sistem tanılama ve optimal ileri besleme kompanzasyonu sunulmuştur. Sıkı referans takibi gereklerine sahip olan bu platformlar, aynı zamanda sürüş hattındaki sürtünme ve boşluk etkileri gibi doğrusal olmayan dinamik etkenlerden yüksek oranda etkilenirler. Doğrusal olmayan dinamik etkilerin giderilerek hassas referans takibi elde etmek amacıyla ilk olarak Eniyi Doğrusal Yaklaşım temelli parametrik olmayan tanılama yöntemleri kullanılmıştır. Sonrasında doğrusal sistem parametrik olmayan sistem modeli üzerinde geri besleme kontrolcü tasarımı gerçekleştirilmiş ve klasik PI döngü şekillendirme senaryoları uygulanmıştır. Üzerine, yüksek mertebeli sinüzoidal girdi tanımlayıcı fonksiyon kavramı temelli, doğrusal olmayan sistem tanılama yöntemleri kullanılarak, hareket platformu üzerinde etkin olan doğrusal olmayan etkenlerin yakalanması amaçlanmıştır. Doğrusal olmayan dinamik etkenlerin ortadan kaldırılması ve hassas referans takibi elde etmek amacıyla, optimal ileri besleme kompanzasyonu tasarımı sunulmuştur. Sistem üzerine uygulanan özel tasarlanmış bir referans sinyali ve Nelder-Mead algoritması ile Stribeck sürtünme modeli tanımlanmıştır. Sonuç olarak önerilen doğrusal olmayan sistem tanılama ve optimal sürtünme giderme yöntemi kullanıldığında, dinamik sistem performansında RMS hız takibi hatası 0.0431 derece/sn'den 0.0117 derece/sn'ye, hız takip hatası integrali standart sapması 0.0382 derece'den 0.0051 dereceye indirilmiştir.

Anahtar sözcükler: Doğrusal olmayan sistemler, İleri beslemeli kontrol, Sistem Tanılama, Sürtünme giderme.

Acknowledgement

I would like to take this opportunity and express my gratitude for everyone who helped me to complete the presented work. First and foremost, I am sincerely grateful to my advisor Onur Özcan for his generous support and inspiration. He has not only guided me in my studies, but also enlightened me throughout my path in academic and personal life.

I would also like to express my deepest appreciation to Zafer Yumrukçal and Mustafa Burak Gürcan for their generous and valuable contribution, and establishing exceptional working environment. I want to appreciate the help of my dear colleagues in ASELSAN, and thank them for their sincere friendship and support. I feel fortunate to have a chance to work alongside those brilliant people.

I want to a pay special tribute to my friends, especially Kerem Şenel, Çağlar Öksüz and Oğuzhan Küçük for their lifelong fellowship and great times we share together. Their comfort and friendship made this long adventure bearable.

My most heartfelt thanks go to my dearest, Gökçe, for believing in me more than I did, and helping me to overcome my hardest times. Thank you for pushing me forward and giving meaning to my life with your light. Like many others, this milestone would not been possible without your existence.

Last but not least, the most credit goes to my parents, Nazan and Ömer, for all the opportunities they provided me, and to my lovely sister, Buse, for being the greatest partner in crime. For each and every success in my life, I owe you a lot. Thank you for your love, everlasting support, patience and everything you have done for me.

Finally, I would like to acknowledge the Presidency of Defence Industries, SSB, for financially supporting this research under SAYP Program No. 82202625-130.10-E.2018-O-19739.

Contents

List of Figures

List of Tables

Chapter 1

Introduction

High precision in motion control systems became an essential performance criteria, as the accuracy definitions have transformed to the micro and even nano levels. Lots of different mechatronics applications are functional with the precise positioning abilities. Various system characteristics and working environments of these devices introduce difficulties in the identification and the control processes with the contribution of the nonlinear effects. In this context, nonlinear system dynamics play a key role in achieving precise motion within the working range of specific engineering applications.

There are a number of systems where small errors due to nonlinear effects cause an intolerable loss in the precision. The intended purpose of the platform defines the bound between tolerable and intolerable precision loss. In general, surveillance systems and camera platforms require higher precision with respect to the remote controlled weapon stations. Even though the frequency response function (FRF) is a strong tool for the frequency domain based identification, most of the crucial nonlinear effects are ignored through linearization around limited range. Hence, the identification and compensation of the nonlinear dynamic effects became essential for the control strategy of corresponding systems.

Earliest system identification methods started with linear approximations of the dynamic systems. Through the assumption of linear time invariant (LTI) systems, identification techniques are comprehensively studied and a considerable amount of instruments became traditional approaches for control community as Prediction Error methods [1], nonparametric and parametric approximations [2, 3], and black-box identification tools [4]. In this extent, frequency domain based system identification techniques like the FRF examined thoroughly for LTI systems in the concept of frequency domain identification [5]. In these applications, it is possible to ignore nonlinear behavior by applying linear identification and control techniques due to insensitive system performance. However, study of nonlinear identification emerges for the cases where nonlinear effects dominate high precision requirements. In order to capture the significant nonlinear dynamics, which are neglected through linear techniques, nonlinear system identification techniques are expanded upon linear strategies [6, 7].

The essential characteristic of LTI systems is the inability to transfer energy in between different frequencies. Therefore, for a sinusoidal input with specific frequency, response is also a sinusoidal with same frequency along with gain and phase shift. In the concept of nonlinear systems, nonlinearities deform the system output by transfering energy from the excited harmonics to other harmonics. The representation of this concept is illustrated in Fig. 1.1. Nonlinear system of $y(t) = cos(u(t)^3)$ is used to illustrate the energy transfer between harmonics.

1.1 Frequency Domain Techniques for Nonlinear Analysis

In order to study the nonlinear behavior of the systems, initial studies in literature utilize Volterra series approximations [8, 9]. Volterra series are generalizing the polynomial approximation of the dynamic systems within limited operating range [10, 11, 12]. Volterra series approximations investigate input-output dynamics of a nonlinear system with harmonic and intermodulation frequency components. It

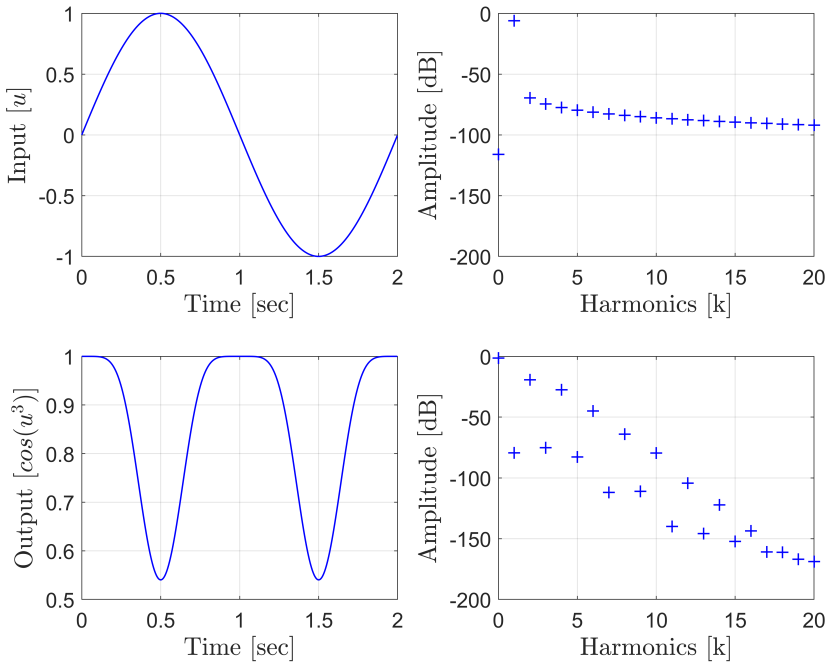

Figure 1.1: Input and output respresentation of nonlinear effects.

is mainly an extension of standard linear convolution definition to the nonlinear study.

For LTI systems, the input-output relation can be described by the convolution integral,

$$y(t) = \int_{-\infty}^{\infty} h(t-\tau)u(\tau)d\tau \tag{1.1}$$

where $u(t)$, $y(t)$ and $h(t)$ are the input, the output and the impulse response function of the linear system, respectively. By taking the Fourier transform of 1.1,

$$Y(w) = H(w)U(w) \tag{1.2}$$

where $U(w)$, $Y(w)$ and $H(w)$ are the Fourier transforms of $u(t)$, $y(t)$ and $h(t)$,

respectively. At this point, $H(w)$ is defined as the Frequency Response Function (FRF) and contains all the information for LTI systems. On the other hand, for nonlinear continuous time-invariant systems with fading memory and under zero initial conditions, if there exist a limited energy input signal $u(t)$, system can be represented by Volterra series approximations [11]. Using Volterra series, response up to order n to an input of $u(t)$ is defined as,

$$y_n(t) = \int_{-\infty}^{\infty} ... \int_{-\infty}^{\infty} h_n(\tau_1, \tau_2, ..., \tau_n) \prod_{m=1}^{n} u(t - \tau_m) d\tau_m \tag{1.3}$$

and

$$y(t) = y_0 + \sum_{n=1}^{\infty} y_n(t) \tag{1.4}$$

where $h_1(\tau)$, $h_2(\tau_1, \tau_2)$, ..., $h_n(\tau_1, \tau_2, ..., \tau_n)$ are the nonlinear extensions of linear impulse response functions, and defined as each order Volterra kernel functions. Based on the mathematical background of the Volterra series approximations, the applications are widely studied containing polynomial, hysteresis and fractional order nonlinear systems [13, 14, 15].

Some other works addressed the generalized frequency response functions (GFRF) with generalization of FRF for nonlinear systems [16, 17, 18, 19]. GFRF is described as multi-dimensional Fourier transform of Volterra kernel function as,

$$H_n(w_1, w_2, ..., w_n) = \int_{-\infty}^{\infty} ... \int_{-\infty}^{\infty} h_n(\tau_1, \tau_2, ..., \tau_n) \prod_{m=1}^{n} e^{-2\pi i \xi_m \tau_m} d\tau_m \tag{1.5}$$

There are also applications with linear approximations in the presence of nonlinearities. Most generalized one is the best linear approximation (BLA) of nonlinear systems along with the idea of nonlinear distortions on FRFs using specialized multi-sine input signals and averaging techniques [20, 21, 22, 23]. When

the nonlinear system is considered as:

$$Y_F(\xi) = B_U(\xi)U_F(\xi) + S_F(\xi) + N_F(\xi) \tag{1.6}$$

where $U_F(\xi)$ and $Y_F(\xi)$ are the input and output, $B_U(\xi)$ is the LTI system, $S_F(\xi)$ is the distortions based on nonlinearities and $N_F(\xi)$ is the output disturbance. Then $B_U(\xi)$ is defined as,

$$B_U(\xi) = \arg\min_{B(\xi)} \mathbb{E}\left\{(y(t) - B(\xi)u(t))^2\right\} \tag{1.7}$$

where $\mathbb{E}\{.\}$ is the ensemble average.

Upon these, idea of nonlinear frequency response functions (NFRF) are investigated in [24]. In this nonlinear case of frequency response function, output spectra depend also on the excitation amplitude along with the excitation frequency. The concept of NFRF generates a nonlinear Bode plots as a moderate approximation of the system gain based on its excitation amplitude and frequency.

$$\mathfrak{B}(w,\gamma) = \frac{1}{\gamma}\left(\sup_{t\in\left[\frac{-\pi}{w},\frac{\pi}{w}\right)} |\mathfrak{N}_o(\mathfrak{N}_s(\mathfrak{s},\mathfrak{c},w))|\right), \tag{1.8}$$

where $\mathfrak{s} = \gamma sin(wt)$, $\mathfrak{c} = \gamma cos(wt)$. $\mathfrak{N}_o(.)$ and $\mathfrak{N}_s(.)$ are the corresponding Nonlinear Output Frequency Response Function (NOFRF) and Nonlinear State Frequency Response Function (NSFRF) [24].

As an alternative concept, the describing function method is utilized to define the dynamic system response to a single sinusoidal signal [25]. Based on the superposition principle of the harmonic responses, describing function method provides approximations of the steady-state solutions to relevant harmonic excitations. Sinusoidal input describing function (SIDF) is defined as,

$$D_s(\xi_0, \gamma) = \frac{Y(\xi_0, \gamma)}{U(\xi_0, \gamma)} \tag{1.9}$$

where u is a sinusoidal input with frequency ξ_0 and amplitude γ. $U(\xi_0, \gamma)$ and $Y(\xi_0, \gamma)$ are the Fourier transforms of $u(t)$ and $y(t)$, respectively.

Depending on the signal and system class, different specialized types of the describing functions are defined such as Generalized Describing Functions (GDF) [26] and Higher Order Sinusoidal Input Describing Function (HOSIDF) [27]. In addition to the mathematical background of sinusoidal input describing function concept, HOSIDF extends the theory to higher harmonics of the response of periodic input by introducing the notion of virtual harmonics generator. Further studies are presented for identification and compensation purposes in [28, 29, 30, 31]. A comprehensive overview for frequency domain methods for nonlinear systems can also be found in [7].

1.2 Goal of the Study

This study originated from the demands of identification and compensation requirements in two-axis gimbal platforms developed at ASELSAN. Due to the precise positioning and reference tracking requirements of the systems, application of nonlinear identification and compensation methodologies is considered as essential.

Scope of the study is based on the need of systematic approach to nonlinear identification and compensation, and to the understanding of the nonlinear effects in an industrial motion platform. Contribution of the work is described based on the functional order of identification process as:

- Study is restricted to a class of time invariant non-linear systems containing harmonic response to a sinusoidal excitation. A standardized method is presented for nonlinear identification and optimal feedforward compensation

of friction characteristics.

- Before investigating the nonlinear behavior, BLA techniques are utilized in order to minimize the effects of nonlinear characteristics to obtain a nonparametric linear model. BLA based nonparametric identification not only provide best approximation of nonlinear system, but also have standardized methodology for the identification process for two-axis gimbal platforms.

- BLA captures nonlinear behaviors based on system characteristics like flexibility, except the dominant friction effect in stick-slip region for our case. Procedure is not limited for a specific type of nonlinearity, but a study of friction compensation in a mechatronic system is discussed for this work using continuous Stribeck friction model [32]. There are other optimal feedforward studies in literature based on the Coulomb [33] and LuGre models [34]. However in order to eliminate the discontinuous characteristics and model dependency, Stribeck model is utilized. Method for friction identification is utilized as a technique with special reference signal and Nelder-Mead Algorithm [35].

- A straightforward procedure for optimal feedforward compensation for a single degree of freedom motion platform is presented by applying the optimal nonlinear control design using HOSIDF based frequency domain identification to reduce nonlinear effects. Optimal case is achieved by decreasing the effect of higher order ($K > 1$) harmonic spectral components Kw_0 ($K \in \mathbb{N}$) to sinusoidal input with frequency w_0.

1.3 Structure of the Thesis

Thesis flow consists of the initial overview of the setup, linear nonparametric identification and feedback controller, nonlinear identification and feedforward compensation, and experimental results. The work done in this thesis is structured as follows.

Chapter 2 gives a brief overview of the experimental setup for nonlinear systems with harmonic responses. By the analytical expansion of the dynamic characteristics of the corresponding system, an introduction to the behavior of the system is presented using the definitions of collocated and noncollocated system responses.

Chapter 3 presents the nonparametric identification of the system, using the conventional frequency response function (FRF) analysis and the Best Linear Approximation (BLA) to different types of excitation input signals separately. By using the nonparametric linear model and classical loop shaping methodology, initial performance criteria are satisfied for best approximation to nonlinear system.

Chapter 4 introduces higher order sinusoidal input describing functions (HOSIDFs) based nonlinear identification and optimal feedforward compensation for the system, in order to eliminate the nonlinear effects and increase the system performance.

Chapter 5 illustrates experimental results and performance evaluations for the test system to conduct a benchmark study, and for a Remote Controlled Weapon System (RCWS), a two degree of freedom gimbal platform to demonstrate the performance of the procedure.

Chapter 2

Experimental Setup and System Analysis

An electromechanical servo subsystem of a rotational motion platform is considered as an identification platform in this study. In order to conduct the identification procedure and verify the results in a practical application, an experimental setup is required. Based on the characteristic driveline in two degree of freedom gimbal systems, essential components of the corresponding rotational motion platform are considered as:

- Motor as a torque source
- Gearbox and/or a pinion - ring gear pair as transmission elements
- Inertial load
- Sensors for angular position, angular speed and applied current

In order to satisfy the requirements of the essential parts in a rotational motion platform, a reference motion platform is selected as experimental setup to conduct benchmark studies. In this chapter, an overview of the motion platform has been

introduced along with the analytic system analysis to briefly introduce the plant dynamics using collocated and noncollocated behaviors.

2.1 Experimental Setup

In order to obtain a comprehensive definition for the desired electromechanical servo subsystem, required components are listed initially. As in the schematics illustrated in Fig. 2.1, electromechanical servo subsystem driveline starts with a servo motor. Rotational motion is transferred from servo motor to the load through a gearbox and an additional pinion-ring gear couple. Each of these components in the driveline has its own stiffness and damping characteristics. Thus, it is complicated to have explicit model for each component in order to obtain the whole system model.

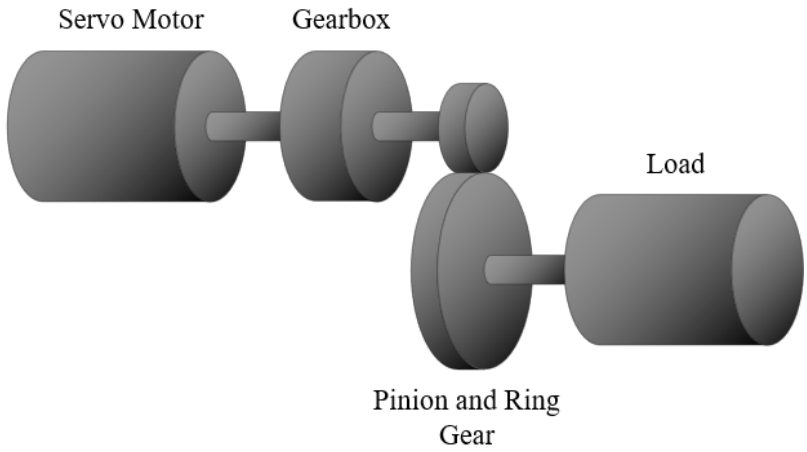

Figure 2.1: Electromechanical servo subsystem driveline for the reference motion platform

With this motivation, an industrial single degree of freedom motion platform shown in Fig.2.2 is selected as an experimental setup. Due to its characteristics, the platform contain all desired parts to be considered as an inclusive platform for an electromechanical servo subsystem driveline in a rotational motion platform. Servo motor is equipped with internal resolver to measure motor shaft angular speed. Load angular speed is also obtained using a mems gyroscope. By this

way, both motor and load side angular speeds are measured using resolver and gyroscope, respectively. Angular position data is collected using encoder, and input current is measured using the current transducer of the motor driver.

In the mechanical design of the test bench, servo motor is originally enabled to rotate around a hinge point. Then it is preloaded with a spring mechanism, which drives pinion against the ring gear in order to maintain minimum backlash for 360°. Whole platform is connected to a stationary stand, and the stand is connected to the ground.

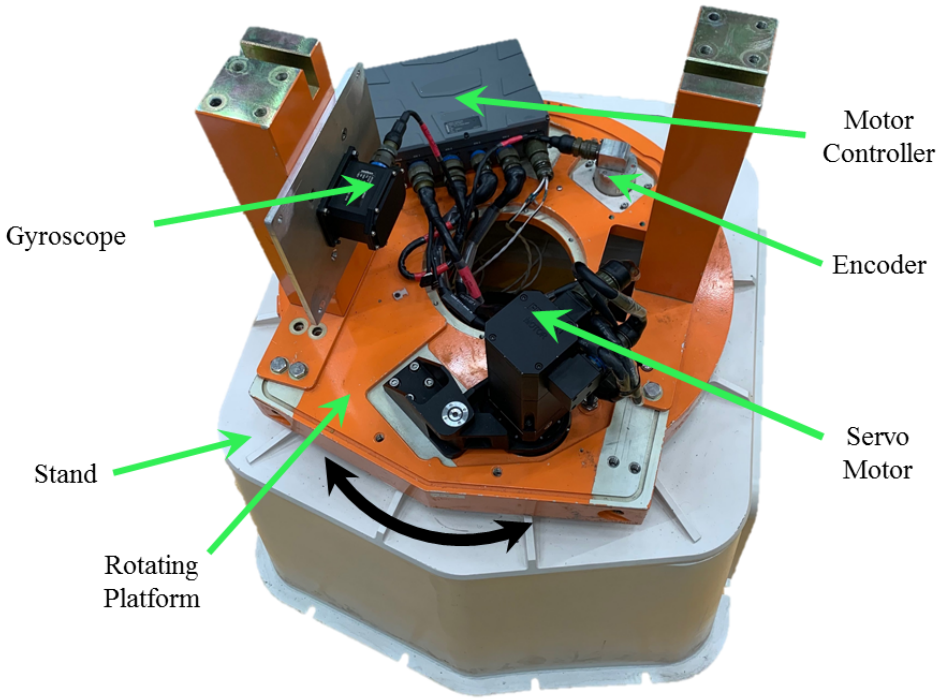

Figure 2.2: Industrial motion platform with one DoF, which is used as experimental test setup.

Overall properties of the setup is presented in Table 2.1. For command input and data logging purposes an external computer is used and data is sampled at 1 kHz.

Table 2.1: Experimental setup properties

Parameter	**Unit**	**Value**
Max. Motor Torque	Nm	3.17
Total Reduction Ratio	$-$	141
Max. Load Speed	deg/s	105
Load Position Measuring Accuracy	deg	0.0055
Motor Speed Measuring Accuracy	deg/s	0.015
Load Speed Measuring Accuracy	deg/s	0.015
Approximated Load Inertia	kgm^2	0.1

2.2 System Analysis

In order to introduce the key concepts in the rotational motion platform dynamics briefly, theoretical approach to the experimental setup is presented in this section. An ideal rotational system consist of motor and load inertias, along with damping and stiffness components. Theoretical system parameters are given in Table 2.2.

Table 2.2: Theoretical system parameters

Parameter	**Unit**	**Symbol**
Motor Shaft Inertia on Load	kgm^2	J_m
Motor Shaft Damping	$Nm/(rad/s)$	c_m
Motor Torque Input	Nm	T_m
Motor Shaft Angular Position	rad	θ_m
Motor Shaft Angular Speed	rad/s	w_m
Transmission Stiffness	Nm/rad	k_s
Transmission Damping	$Nm/(rad/s)$	c_s
Load Inertia	kgm^2	J_l
Load Damping	$Nm/(rad/s)$	c_l
Disturbance Torque	Nm	T_d
Load Angular Position	rad	θ_l
Load Angular Speed	rad/s	w_l

Figure 2.3 shows the described driveline in an electromechanical servo subsystem of rotational platform.

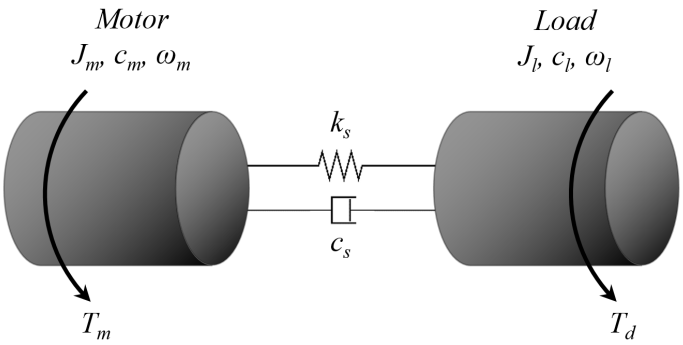

Figure 2.3: System representation with motor-load inertias and elastic driveline of the rotational platform.

In order to describe the dynamic behavior of the system in the context of collocated and noncollocated dynamics, equations of motion (EoM) are written as eqns. 2.1 and 2.2. Transmission ratio is not included to the equations, since motor inertia is defined in the load side by multiplying with the square of transmission ratio.

$$T_m(t) - J_m\ddot{\theta}_m(t) - c_m\dot{\theta}_m(t) - k_s(\theta_m(t) - \theta_l(t)) - c_s(\dot{\theta}_m(t) - \dot{\theta}_l(t)) = 0 \qquad (2.1)$$

$$T_d(t) - J_l\ddot{\theta}_l(t) - c_l\dot{\theta}_l(t) + k_s(\theta_m(t) - \theta_l(t)) + c_s(\dot{\theta}_m(t) - \dot{\theta}_l(t)) = 0 \qquad (2.2)$$

If the system is considered as Linear Time Invariant (LTI), eqns. 2.1 and 2.2 can be transformed using the Laplace transformation. In this content, the motor torque T_m and disturbance torque T_d are considered as input variables, where the angular speeds of motor w_m and load w_l are considered as output variables of the EoM.

$$(J_m s + c_m + \frac{k_s}{s} + c_s)w_m(s) - (\frac{k_s}{s} + c_s)w_l(s) = T_m(s) \tag{2.3}$$

$$(J_l s + c_l + \frac{k_s}{s} + c_s)w_l(s) - (\frac{k_s}{s} + c_s)w_m(s) = T_d(s) \tag{2.4}$$

By solving eqns. 2.3 and 2.4, transfer functions from motor torque T_m to motor angular speed w_m and load angular speed w_l can be written as:

$$\frac{w_m(s)}{T_m(s)} = \frac{J_l s^2 + (c_l + c_s)s + k_s}{s\left[(J_m s + c_m + \frac{k_s}{s} + c_s)(J_l s + c_l + \frac{k_s}{s} + c_s) - (\frac{k_s}{s} + c_s)(\frac{k_s}{s} + c_s)\right]} \tag{2.5}$$

$$\frac{w_l(s)}{T_m(s)} = \frac{c_s s + k_s}{s\left[(J_m s + c_m + \frac{k_s}{s} + c_s)(J_l s + c_l + \frac{k_s}{s} + c_s) - (\frac{k_s}{s} + c_s)(\frac{k_s}{s} + c_s)\right]} \tag{2.6}$$

These transfer functions represent the dynamic behavior for ideal driveline with two inertias, along with stiffness and damping characteristics. Bode diagrams for a theoretical sample system are given in Fig. 2.4a for motor side, and 2.4b load side. In this case, system with motor shaft inertia on load $J_m = 0.1\ kgm^2$, load inertia $J_l = 0.5\ kgm^2$, transmission stiffness $k_s = 5000\ Nm/rad$ and transmission damping $c_s = 0.01 - 1 - 5 - 10\ Nm/(rad/s)$ is considered. For the ideal driveline, c_m amd c_l are set to zero.

Bode diagrams in Fig. 2.4a and 2.4b indicates the corresponding resonant and anti-resonant frequency characteristics for a theoretical system. In a real application, more than one resonant and anti-resonant couples can be observed due to the complexity of the system. Such systems can also be modeled as the resultant dynamics of the second order systems connected in parallel. Thus, the minimum system order of the parametric models can be obtained from the number of resonant and anti-resonant couples in the complex systems. Moreover, a phase is observed in low frequency due to the selected input-output pair as torque and speed.

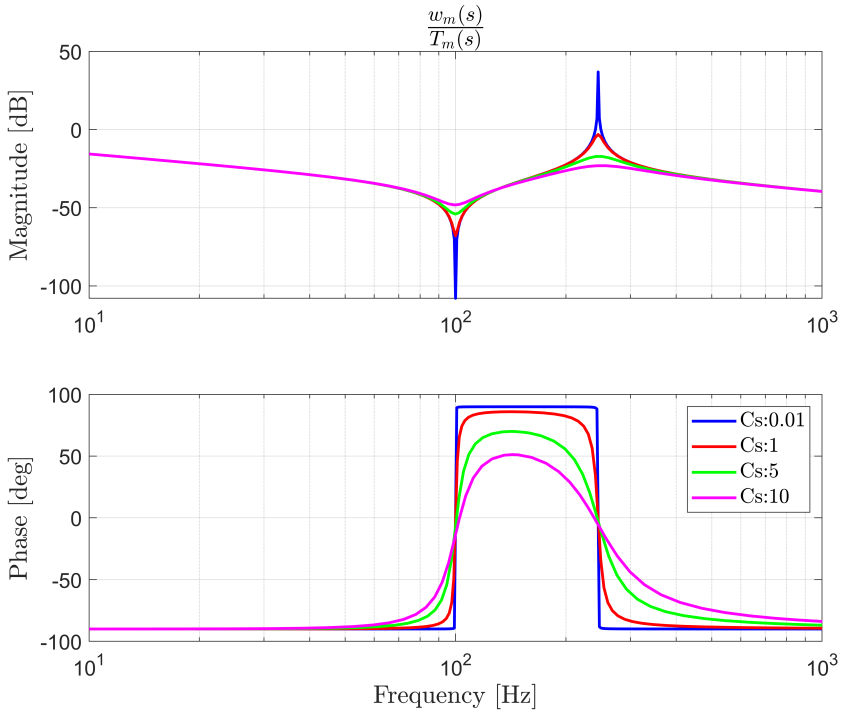

(a)

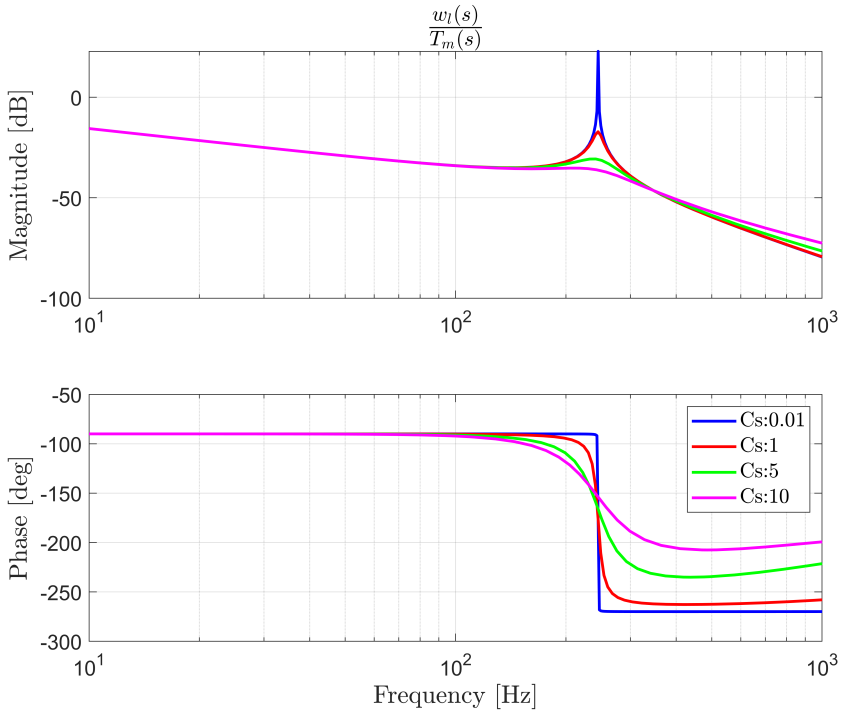

(b)

Figure 2.4: Motor and load side bode diagrams for the sample theoretical system.

Chapter 3

Nonparametric Identification of Nonlinear Systems

The nonparametric model representation of a dynamic system can be considered as a quantitative characterization of the system using measurements of the frequency response at various frequencies. In this standardized concept, system is not defined with the aid of finite number of parameters and there are no connections between the measurements at different frequencies. In this chapter, nonparametric identification of a class of nonlinear systems is discussed. Initial discussion is focused on the conventional frequency response function analysis of the system in order to create a benchmark approach to the concept. Then, Best Linear Approximation method is presented for the class of nonlinear system which is defined as PISPO (period in, same period out) systems. In both conventional FRF and BLA scenarios, specialized excitation signals are discussed for the corresponding context.

The dynamic characteristics of the system is mainly based on the measurements of the input and the output signals. Therefore, the design of the excitation signal for system identification process can be considered as a crucial component. In the early times of the system identification, the swept sine input along with a tracking filter was extremely common excitation signal type [5]. Due to the

enhancement of the digital signal processing environments, more advanced input signals and techniques are utilized as identification tools. Instead of exciting each frequency independently, complex excitation signals containing broadband spectrum are used, along with the reduced measurement time. Different concepts of excitation signals are are used in literature such as broadband random, sine, step or transient signals.

In the parametric model representation of a dynamic system, the energy contribution of different frequencies to the excitation signal should be concentrated at particular frequencies where the contribution to the model parameters are in considerable level. However, in the nonparametric model representation, input signal is aimed to satisfy an accuracy limit in the corresponding frequency range. Therefore, in order to obtain an optimized excitation signal, uncertainty on the FRF is considered. It is dependent on the characteristics of the power spectrum of the excitation signal and its total power. To achieve a constant variance in the range of frequency band, the disturbing noise impact became important. In this context, crest factor is defined as a comprehensive quality factor in eqn. (3.1). It is defined as the ratio of the peak value u_{peak} to rms value u_{rms} of the input signal $u(t)$.

$$Cr(u) = \frac{u_{peak}}{u_{rms}} = \frac{\max_{t\in[0,T]} \mid u(t) \mid}{u_{rms}\sqrt{P_{int}/P_{tot}}} \text{ with } u_{rms}^2 = \frac{1}{T}\int_0^T u^2(t)dt \qquad (3.1)$$

where T is the measurement time, P_{tot} and P_{int} are the total power and power in frequency band of interest, respectively. Crest factor is a measure for the compactness for an input signal. Smaller values of a crest factor defines a good quality of the excitation signal.

In order to obtain the system behavior in a single measurement, special broadband excitation signal can be utilized, instead of exciting each frequency independently. A number of different general purpose broadband excitation signals are investigated for this study.

3.1 Conventional Frequency Response Function

Conventional Frequency Response Function (CFRF) approach is initially studied by using particular measurements for each frequency. Taking measurements frequency by frequency and using a descriptive tool for each frequency point enables to obtain a nonparametric system model for a given frequency band. In order to separate each frequency step, swept sine excitation signal is applied. Then, FFT tools are utilized in order to extract the gain and phase information for each frequency step. CFRF approach described in this section has been utilized as an underlying technique for many years in both literature and industry in identification of the mechatronic systems.

3.1.1 Excitation Signal

As one of the most common excitation signals, swept sine excitation is defined as a sine sweep input signal where the frequency of the excitation is swept up or down in one measurement period [36].

$$u(t) = A\sin(((\pi(k_2 - k_1)f_0^2)t + 2\pi k_1 f_0)t) \text{ where } 0 \leq t < T_0 \tag{3.2}$$

where T_0 is the period, $f_0 = 1/T_0$, $k_2 > k_1 \in \mathbb{N}$, and $k_1 f_0$ and $k_2 f_0$ are the lowest and the highest frequency, respectively. Due to its nature, swept sine signal is a periodic signal with a frequency resolution of $1/T_0$. The excitation power is generally equally distributed in the selected frequency band defined with k_1 and k_2. The swept sine torque input signal and the load-motor speed output signal is presented in Fig. 3.1a. For the excitation signal used in experimental setup, k_1, k_2 and A are selected as 1, 100 and 0.6, respectively, with a frequency step size of 0.5 Hz. For each frequency, the input signal is created for 16 cycles in order to enable transient effects to be eliminated. Figure 3.1b illustrates the detailed view of the input and output signals.

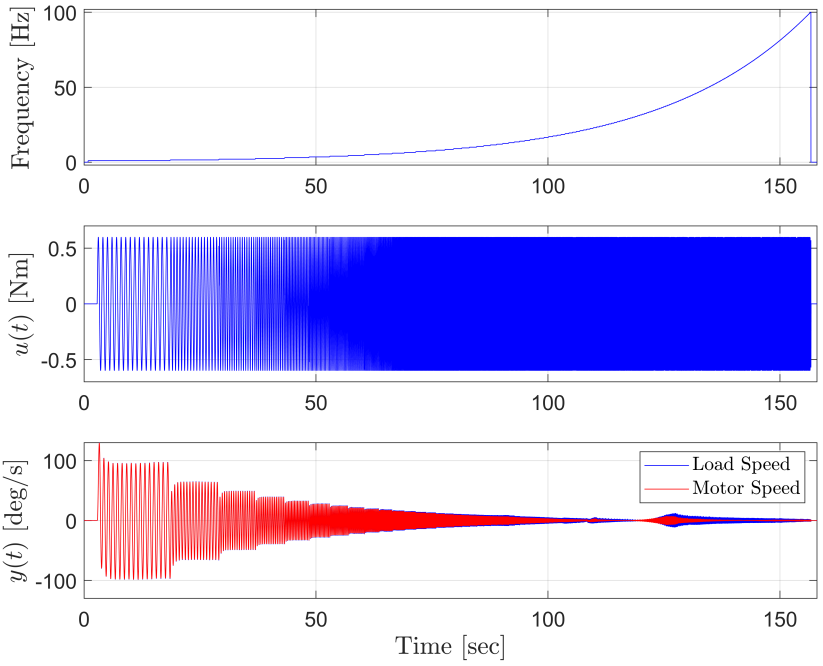

(a)

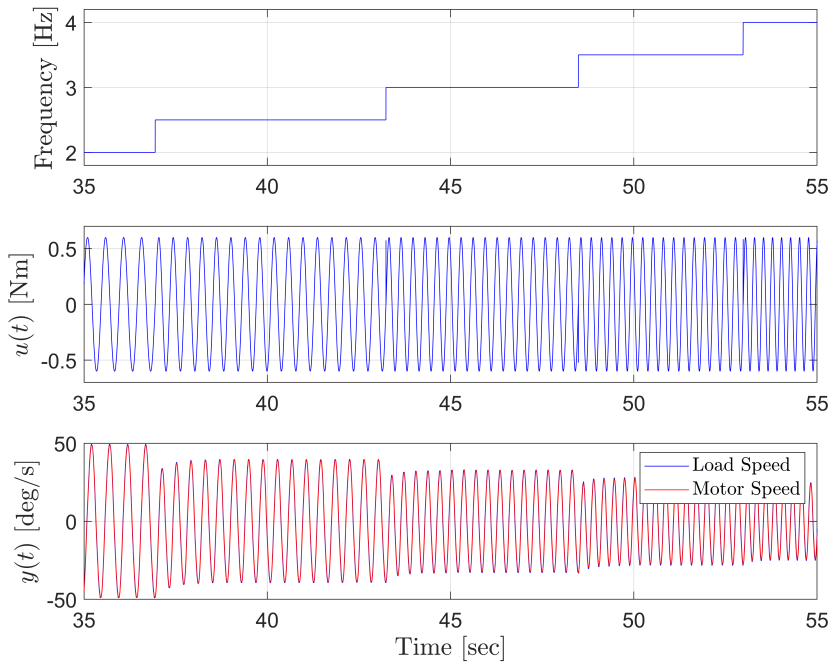

(b)

Figure 3.1: The swept sine periodic excitation signal and the plant response (a), detailed view (b).

Its crest factor, which is 1.41, is considerably low. However, low SNR frequency components are included due to the amplitude spectrum characteristics of the swept sine signal. Hence, to achieve a certain level of accuracy, the measurement time should be longer. Besides, it is not only exciting the desired frequency but also couple of other spectral components, leading to errors in nonlinear systems.

3.1.2 Methodology

After obtaining the measurements with the swept sine excitation signal, measurement is used for the exact frequency information for every instant. Although there are 16 cycles in each frequency, first cycles are omitted to eliminate the transient effects observed after frequency changes. Then, frequency domain signals are obtained using FFT from the corresponding time domain signals for each frequency. The frequency response function are defined as:

$$\hat{G}(jw_k) = \frac{\max_{w\in[1,L]}(Y(jw))}{U(jw_k)} \tag{3.3}$$

for frequency f_k where $k = 1, 2, ..., L$ for a desired interval of frequencies. Instead of frequency by frequency identification, maximum value of the output spectra is used in the nonparametric model in order to obtain better representation of the nonparametric model. Moreover, windowing can minimize the effects of FFT and achieve better nonparametric models in this content.

3.1.3 Experimental Results

Using input and output measurements presented in Fig. 3.1a and defined methodology, CFRF of the experimental setup is obtained for the motor and the load side, and presented in Fig. 3.2a and Fig. 3.2b, respectively. As in Fig. 3.2b, the load side results does not clearly represent a noncollocated behavior due to the fact that the measurement point is not exactly the end point of the structure.

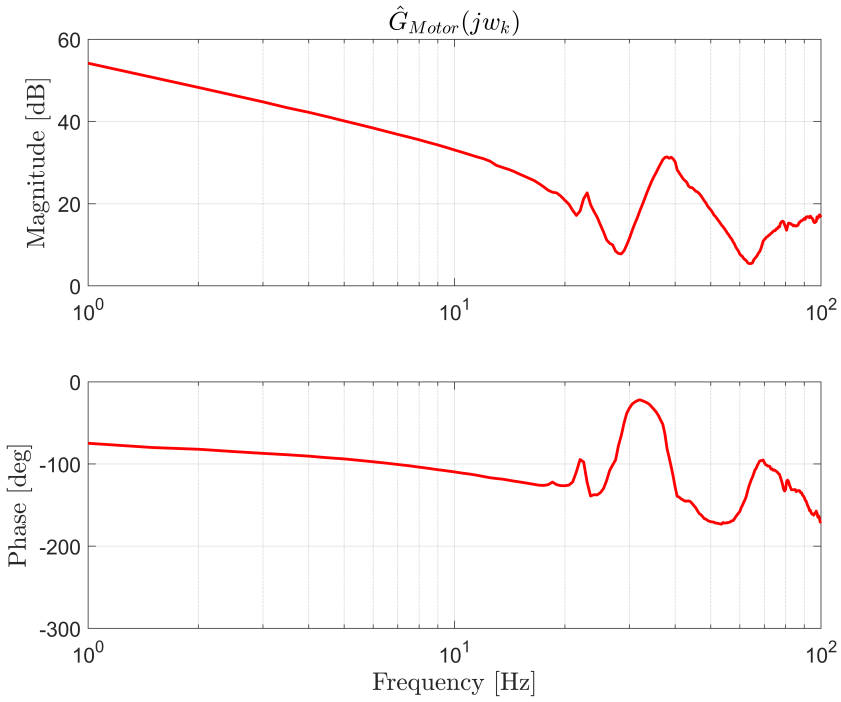

(a)

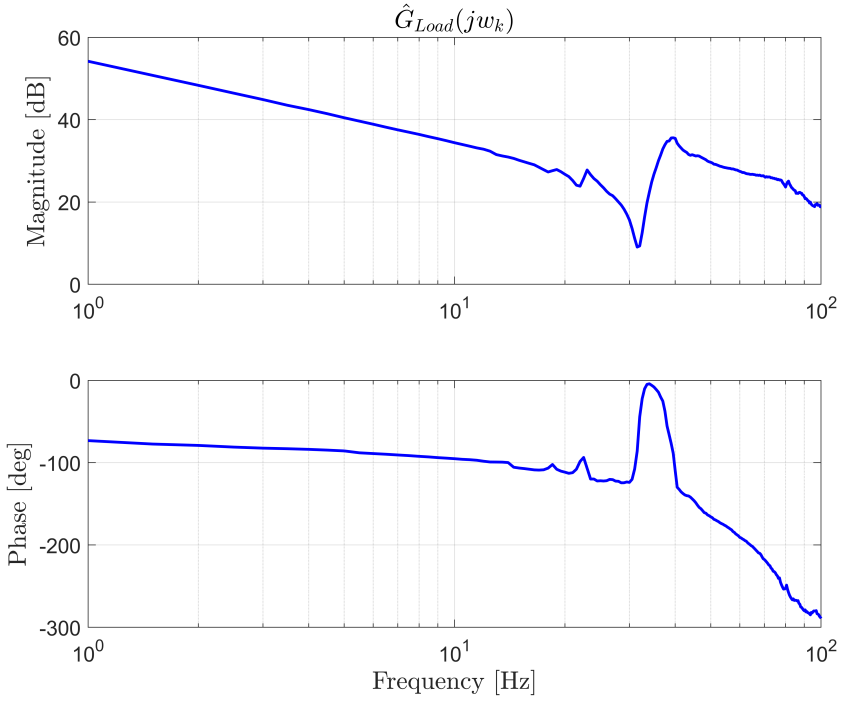

(b)

Figure 3.2: The nonparametric identification using conventional FRF tools from the input torque to the output speed of the motor (a), and the load (b).

3.2 Best Linear Approximation

Best Linear Approximation (BLA) is described as a descriptive tool for the identification of nonlinear systems. In many cases, the nonlinear distortions generally observed in lower magnitude levels compared to the linearized models. In the representation of Best Linear Approximation, the nonlinear distortions are defined as an additional term to the output of linear system [5]. The schematic representation of a nonlinear system and equivalent best linear approximation is illustrated in Fig. 3.3 as referred in eqn. 1.6.

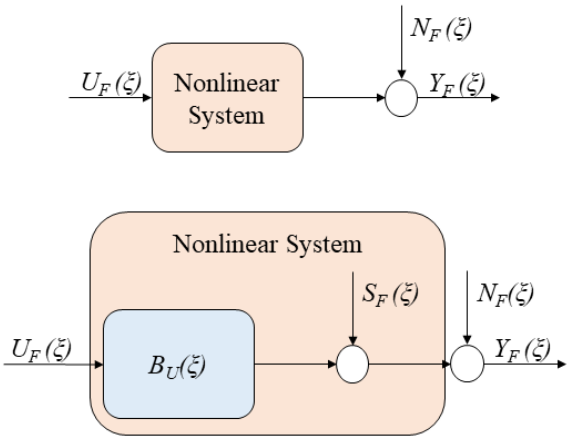

Figure 3.3: The representation of the nonlinear system output by BLA and stochastic nonlinear terms where $B_U(\xi)$ is the LTI system, $S_F(\xi)$ is the distortions based on nonlinearities and $N_F(\xi)$ is the output disturbance.

3.2.1 Excitation Signal

In contrast of conventional FRF methodology, Best Linear Approximation utilizes much compact excitation signals within shorter measurement times. Therefore, design of excitation signal gains more importance. For the given time of measurement, information from the system should be retrieved as much as possible. Therefore, potential excitation signals are considered as an input signal namely random noise excitation and random phase multisine excitation.

3.2.1.1 Random Noise Excitation

Random noise excitation signals are highly utilized in different practical applications of identification methods due to their characteristic behaviors. The frequency resolution and the amplitude spectrum of the input noise signal are determined by the length of the experiment and the noise shaping signals, respectively. In order to obtain a considerable model using the random noise excitation signal, a number of realizations are required. Increasing the number of realizations and averaging between these realizations enable user to obtain defined amplitude spectrum as shown in Fig. 3.4. An additional shaping filter can be utilized in order to transform the random noise into a Gaussian distribution. User defined power and amplitude spectrum can also be generated using different procedures [37].

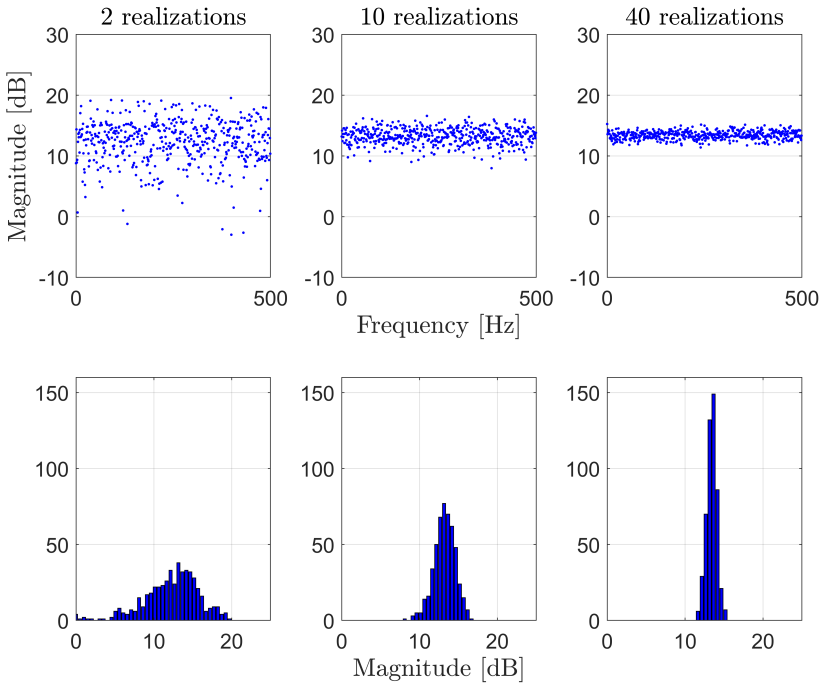

Figure 3.4: Spectrums of the random noise excitations with different number of realizations.

3.2.1.2 Random Phase Multisine Excitation

The zero mean random phase multisine excitation signal is defined as:

$$u(t) = \sum_{k=-N/2+1, k\neq 0}^{N/2-1} U_k e^{j2/pif_s kt/N} \tag{3.4}$$

where the Fourier coefficients U_k are either zero or meet the requirements of $|U_k| = \hat{U}(kf_s/N)/\sqrt{N}$. Based on the selection of excited harmonics, different types of the excitation signals are defined. The full random phase multisine excites all harmonics where the odd random phase multisine excites all odd harmonics in the defined frequency band. Furthermore, the random phase multisine with random harmonic grid excites randomly selected harmonics within each group of successive harmonics N_{sub}. Harmonic contents of different random phase multisine excitation signals are presented in Fig. 3.5.

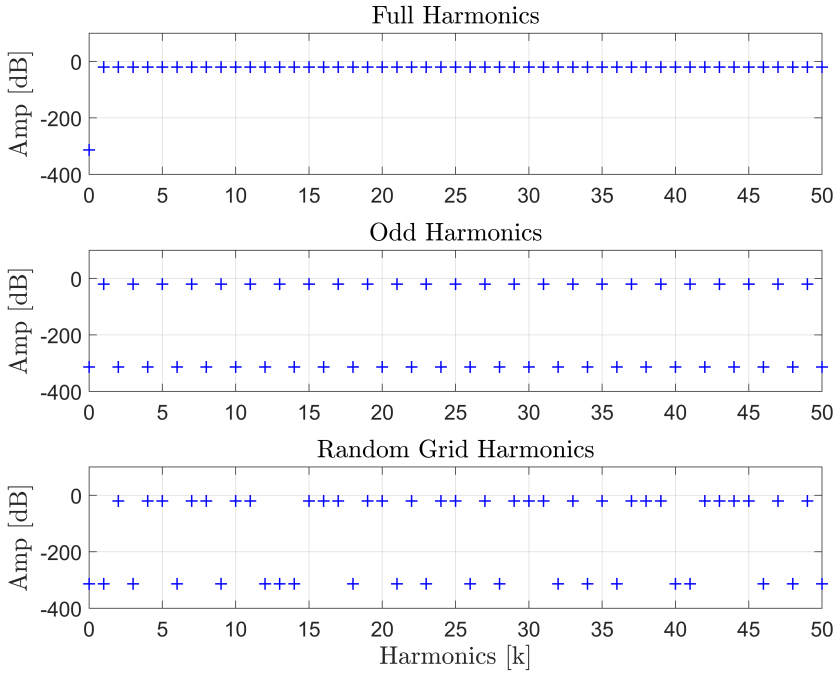

Figure 3.5: Harmonic contents of different random phase multisine excitation signals.

3.2.2 Methodology

In order to understand the influence of the nonlinear system characteristics on frequency response function (FRF) measurements, properties of nonlinear systems should be discussed. In this point, the definitions for static and dynamic nonlinear systems should be addressed.

The response $y(t)$ of a LTI system to a periodic input $u(t)$ is again a periodic output with the same period as the input. For the static nonlinear systems, the response contains energy on the output, not only in the frequency of the input signal but also in other frequencies. It is impossible for LTI systems to transfer energy from the input frequency to other frequencies.

For the dynamic nonlinear system, the discussion can be restricted to a class of dynamic nonlinear systems, which can be estimated well with a Volterra series mean square approximations on a given input domain. This class of nonlinear systems enable to describe nonlinear phenomena like friction or backlash as in our case of study. Therefore, the analysis for the dynamic nonlinear systems can be considered as restricted to the class of dynamic nonlinear system, which can be defined as PISPO (period in, same period out). This restriction ignores the nonlinear behaviors of subharmonics, bifurcation and chaos [37].

To obtain a nonparametric model for the defined class of dynamic nonlinear systems, best linear approximation method is a commonly used method in literature. The best linear approximation of for a class of nonlinear system minimizes the mean square error between the true output of the nonlinear system and the output of the linear model. DC values of the input and output signals are removed from the measurements and the measurement of the impulse response $g(t)$ of a linear system defined in the concept of correlation analysis. For an input signal of $u(t)$ and output signal of $y(t)$:

$$R_{yu}(t) = g(t) * R_{uu}(t) \tag{3.5}$$

where $*$ is the convolution product, $R_{uu}(t)$ and $R_{yu}(t)$ are the autocorrelation and the crosscorrelation, respectively, defined as Wiener-Hopf equation.

$$R_{uu}(\tau) = \mathbb{E}\{u(t)u(t-\tau)\} \text{ and } R_{yu}(\tau) = \mathbb{E}\{y(t)u(t-\tau)\} \tag{3.6}$$

For a random excitation signal, the solution of eqn. 3.5, with respect to $g(t)$, minimizes to

$$\mathbb{E}\{\|y(t) - g(t) * u(t)\|^2\} \tag{3.7}$$

By taking the Fourier transform of 3.5, relation for the nonparametric model is obtained as:

$$G(jw) = \frac{S_{YU}(jw)}{S_{UU}(jw)} \tag{3.8}$$

where the frequency response function $G(jw)$, the auto-power spectrum $S_{UU}(jw)$ and the cross-power spectrum $S_{YU}(jw)$ are the Fourier transforms of $g(t)$, $R_{uu}(t)$ and $R_{yu}(t)$, respectively [38, 39]. In the defined class of dynamic nonlinear systems with weak nonlinear behavior, linear approximations to the nonlinear system can be obtained. By removing the mean values of the input and output signals, eqn. 3.7 can be written as

$$\mathbb{E}\{\|\tilde{y}(t) - g(t) * \tilde{u}(t)\|^2\} \tag{3.9}$$

where

$$\tilde{u}(t) = u(t) - \mathbb{E}\{u(t)\} \text{ and } \tilde{y}(t) = y(t) - \mathbb{E}\{y(t)\} \tag{3.10}$$

In order to utilize the finite time input and output measurements, eqn. 3.8 is estimated as

$$\hat{G}_{BLA}(jw_{k+1/2}) = \frac{\hat{S}_{YU}(jw_{k+1/2})}{\hat{S}_{UU}(jw_{k+1/2})} = \frac{\frac{1}{M}\sum_{m=1}^{M} Y_{diff}^{[m]}(k)\overline{U_{diff}^{[m]}}(k)}{\frac{1}{M}\sum_{m=1}^{M}\left|U_{diff}^{[m]}(k)\right|^2} \tag{3.11}$$

and the variance of the BLA is approximated as

$$\mathrm{var}(\hat{G}_{BLA}(jw_{k+1/2})) = \frac{1}{M-1}\frac{\hat{S}_{YY}(jw_{k+1/2}) - \left|\hat{S}_{YU}(jw_{k+1/2})\right|^2 / \hat{S}_{UU}(jw_{k+1/2})}{\hat{S}_{UU}(jw_{k+1/2})} \tag{3.12}$$

with M realizations and N samples for each realization, and $X^{[m]}(k)$ is the DFT spectrum of m^{th} realization which is

$$X^{[m]}(k) = \frac{1}{\sqrt{N}}\sum_{t=0}^{N-1} x((m-1)N+t)e^{-2\pi jkt/N} \tag{3.13}$$

Difference operation $X_{diff}(k) = X(k+1) - X(k)$ are implemented in order to avoid leakage errors which approximates to zero as N goes to infinity. In order to reduce the variance on best linear approximation and obtain accurate $\hat{G}_{BLA}(jw_{k+1/2})$, number of realizations M should be increased. In the ideal case of M and N approaches to infinity, eqn. 3.11 and 3.12 converges to eqn. 3.8 and zero, respectively.

For a periodic excitation signal, eqn. 3.8 is re-written as

$$G_{BLA}(jw) = \frac{S_{YU}(jw)}{S_{UU}(jw)} = \frac{\mathbb{E}\{Y(k)\overline{U}(k)))\}}{\mathbb{E}\{|U(k)|^2\}} = \frac{\mathbb{E}\{Y(k)\overline{U}(k)))\}}{|U(k)|^2} = \mathbb{E}\left\{\frac{Y(k)}{U(k)}\right\} \tag{3.14}$$

Similar to random excitation, for M realizations of random phase multisine, eqn. 3.14 is approximated as

$$\hat{G}_{BLA}(jw_{k+1/2}) = \frac{1}{M}\sum_{m=1}^{M}\frac{Y^{[m]}(k)}{U^{[m]}(k)} \tag{3.15}$$

and its variance estimated as

$$\mathrm{var}(\hat{G}_{BLA}(jw_{k+1/2})) = \frac{1}{M(M-1)}\sum_{m=1}^{M}\left|\frac{Y^{[m]}(k)}{U^{[m]}(k)} - \frac{1}{M}\sum_{m=1}^{M}\frac{Y^{[m]}(k)}{U^{[m]}(k)}\right|^2 \tag{3.16}$$

Due to the random characteristics of the multisine input, the variability of the BLA increases. Hence, number of realizations M should be higher in order to obtain an estimate with good accuracy. Similar to the random noise input scenario, as M and N approaches to infinity, eqn. 3.15 and 3.16 converges to eqn. 3.14 and zero, respectively.

As a result, for the input and output measurements without errors, obtained BLA can be concluded as

$$\hat{G}_{BLA}(jw_k) = G_0(jw_k) + G_B(jw_k) + G_S(jw_k) \tag{3.17}$$

where $G_S(jw_k)$ is defined as "nonlinear noise source" with $\mathbb{E}\{G_S(jw_k)\} = 0$ and $G_B(jw_k)$ is defined as "nonlinear bias contribution source". The power spectrum and the probability density function (pdf) of the excitation signal have a considerable influence on the characteristics of $G_S(jw_k)$. Hence, $G_S(jw_k)$ can be reduced by increasing the number of realizations M. Consequently, estimations of best linear approximation can be introduced as

$$\hat{G}_{BLA}(jw_k) = (G_0(jw_k) + G_B(jw_k) + O_B(N^{-1})) + (G_S(jw_k) + O_s(N^{-1/2})) \tag{3.18}$$

In this context, $O_B(N^{-1})$ is defined as the bias term arised from the leakage errors in noise inputs and finite number of corresponding frequencies in the random phase multisine inputs. It can be reduced by increasing the period or block lenght N. $O_s(N^{-1/2})$ is defined as the stochastic term due to leakage errors in noise inputs. Stochastic term is zero by its nature in the random phase multisine inputs with $\mathbb{E}\{O_s\} = 0$. It can be reduced by increasing M and/or N.

3.2.3 Experimental Results

The input and output measurements are conducted for the cases of input signal with (i) Gaussian white noise, (ii) Full harmonic random phase multisine, (iii) Odd harmonic random phase multisine and (iv) Random grid harmonic phase multisine, separately. The input and output signals are presented for each input signal in Fig. 3.6a and Fig. 3.6b, respectively. Crest Factor of the input signal is 3.57 for (i) Gaussian white noise, 3.55 for (ii) Full harmonic multisine, 2.74 for (iii) Odd harmonic multisine and 2.99 for (iv) random grid harmonic multisine. When the only input signal is noise or multisine, system behavior is mostly dominated by the friction and the backlash. In order to minimize the nonlinear friction and backlash effects in this step, a square torque signal is added to excitation signals for each case. Therefore, output measurements differs from zero crossing regions. Due to the fact the chosen excitation signals and square torque signal is statistically independent from each other, only the excitation signal can be considered as input for the methodology of BLA. This property of statistically independent signals guarantee the fact that they have no influence on each others approximated linear model.

Nonparametric models for the motor and the load speed output are obtained using BLA methodology similar to the conventional FRF. BLA results are presented with conventional FRF results in Fig. 3.7a and Fig. 3.7b for (i) Gaussian white noise, Fig. 3.8a and Fig. 3.8b for (ii) Full random phase multisine, Fig. 3.9a and Fig. 3.9b for (iii) Odd random phase multisine, and Fig. 3.10a and Fig. 3.10b for (iv) random grid harmonic phase multisine excitation signals.

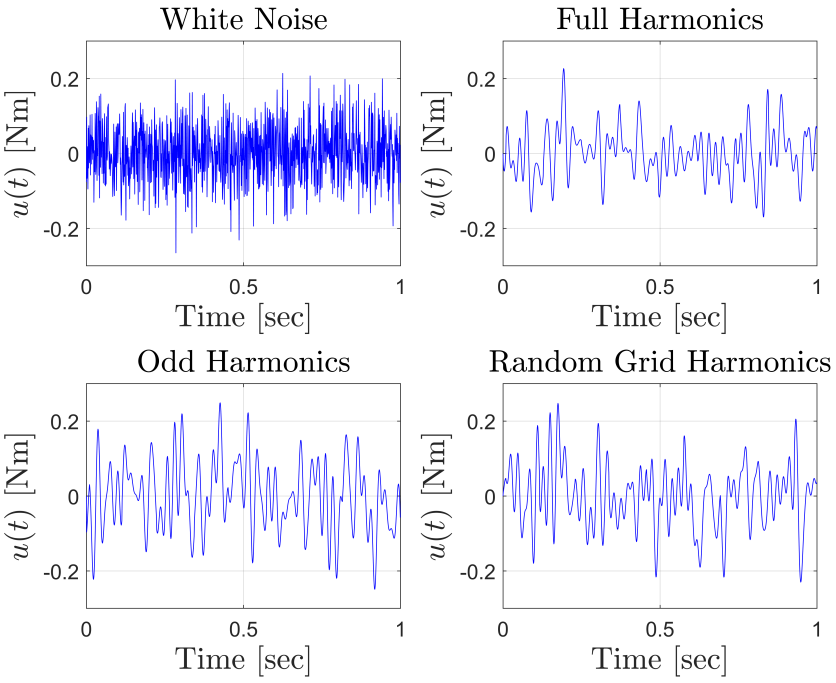

(a)

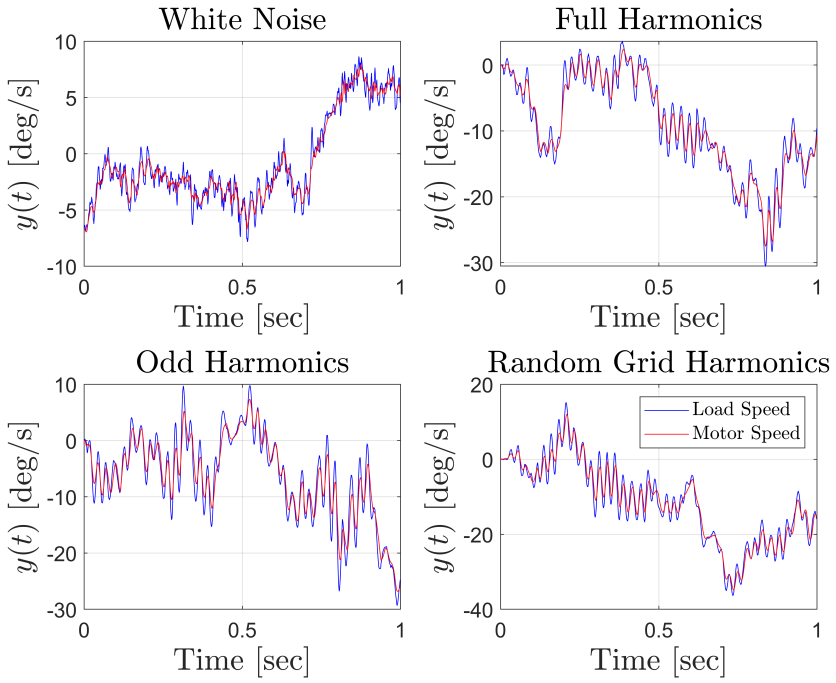

(b)

Figure 3.6: The excitation input signal (a) and the output signal (b) measurements for Best Linear Approximation.

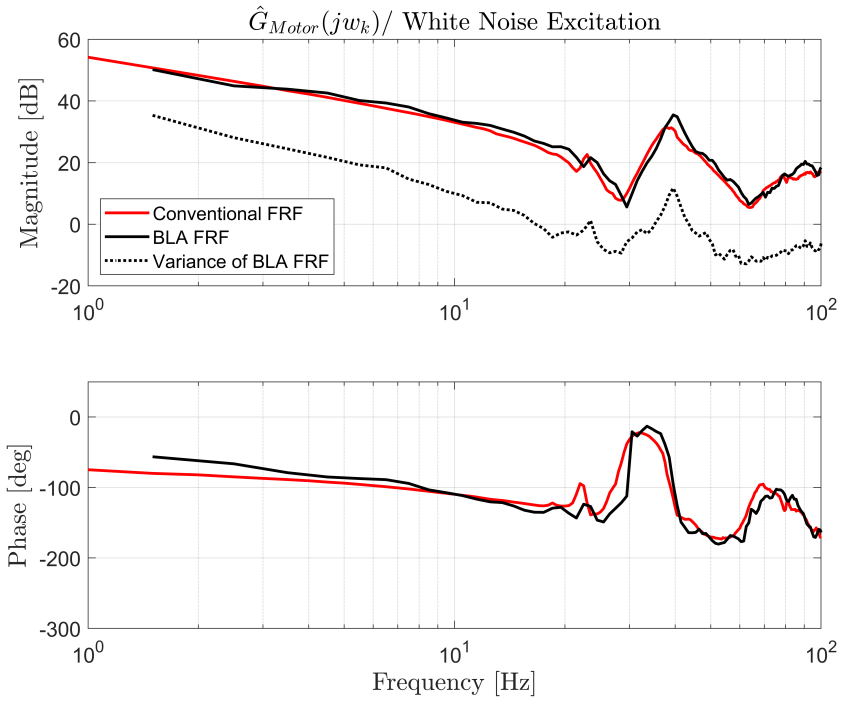

(a)

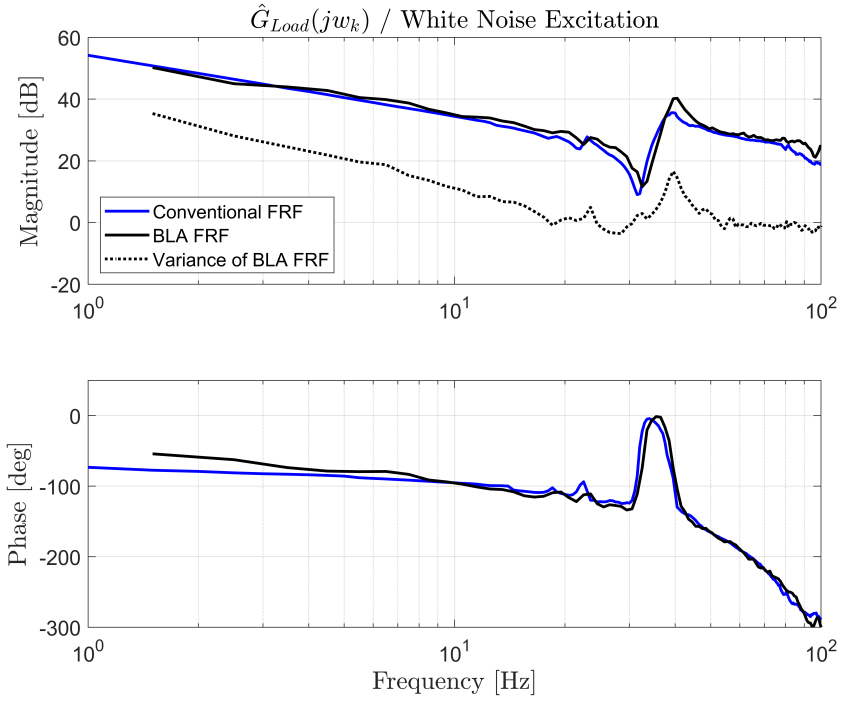

(b)

Figure 3.7: The nonparametric model obtained using BLA from torque input to motor speed output (a), and load speed output (b) with the white noise excitation.

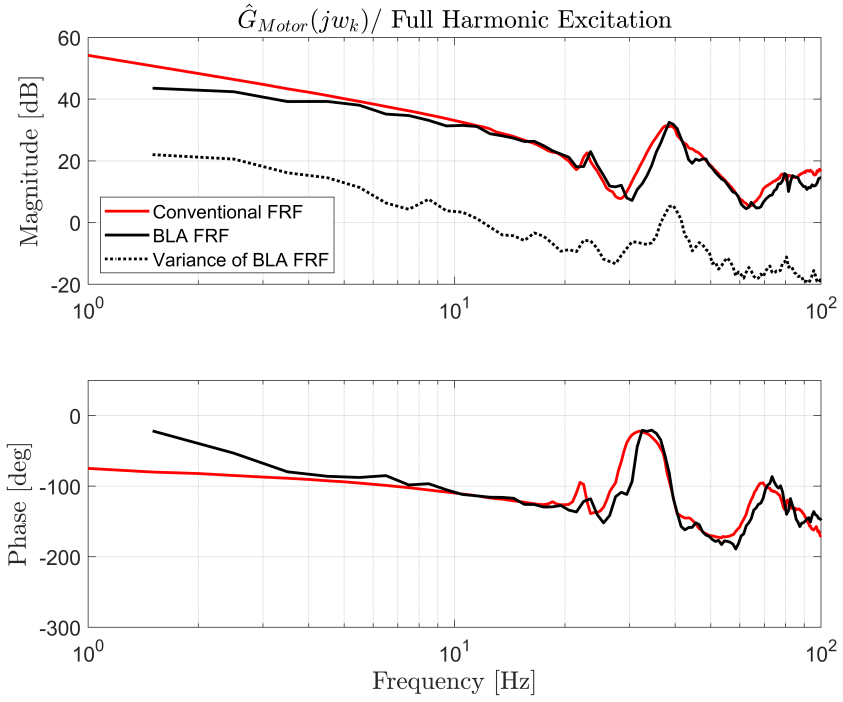

(a)

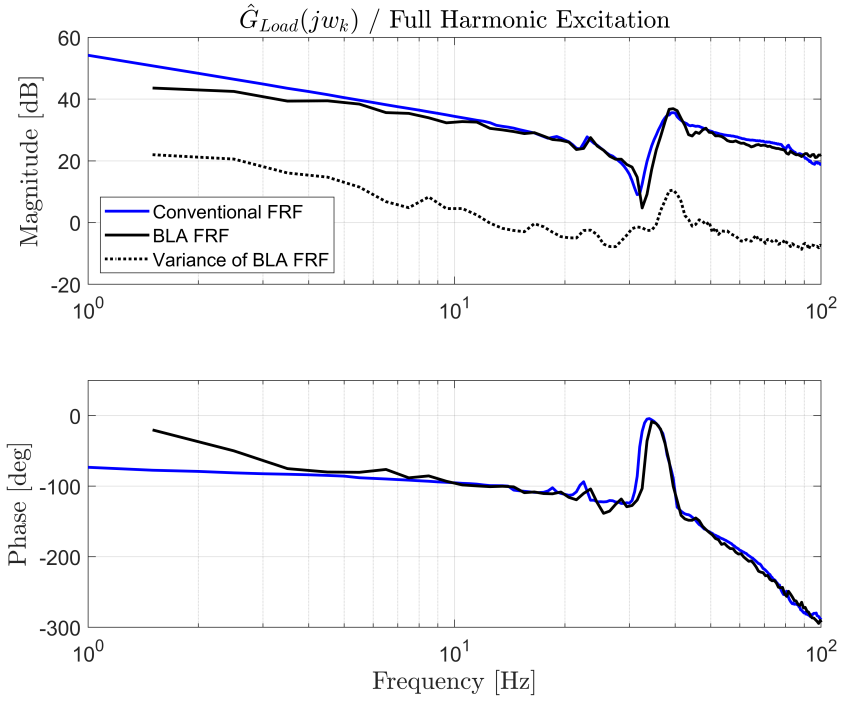

(b)

Figure 3.8: The nonparametric model obtained using BLA from torque input to motor speed output (a), and load speed output (b) with the full harmonic random phase multisine excitation.

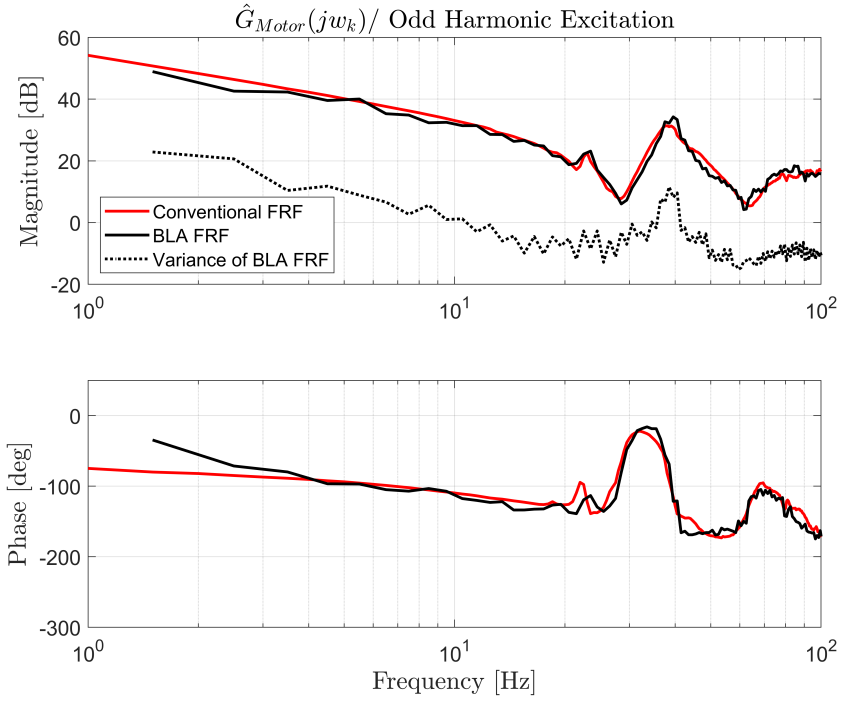

(a)

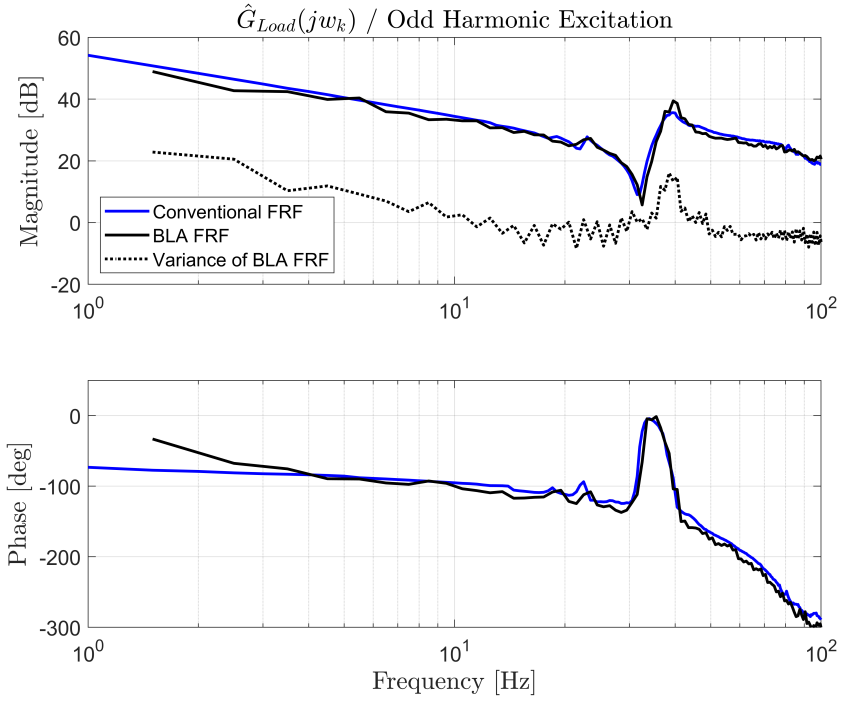

(b)

Figure 3.9: The nonparametric model obtained using BLA from torque input to motor speed output (a), and load speed output (b) with the odd harmonic random phase multisine excitation.

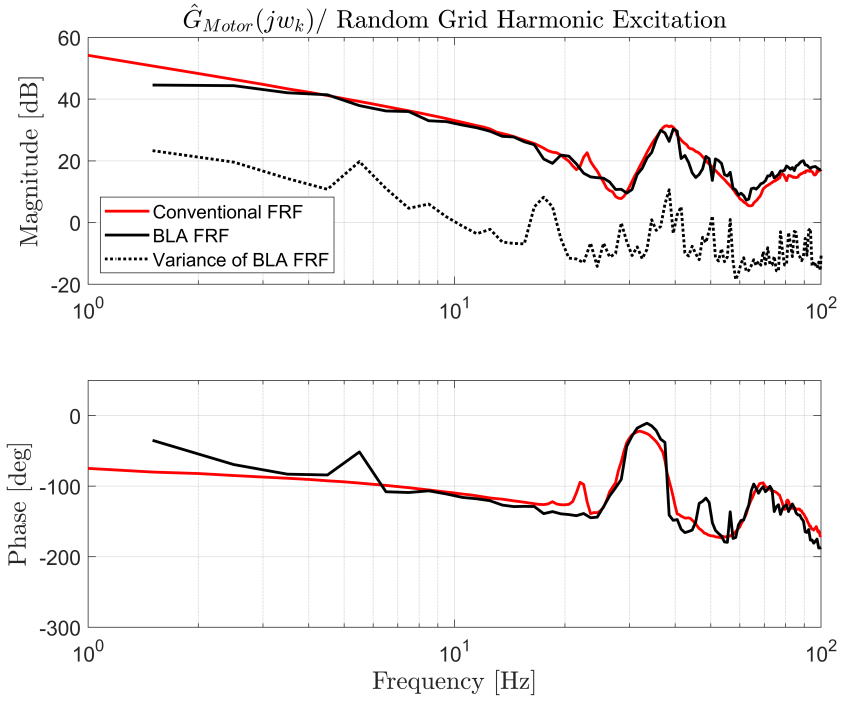

(a)

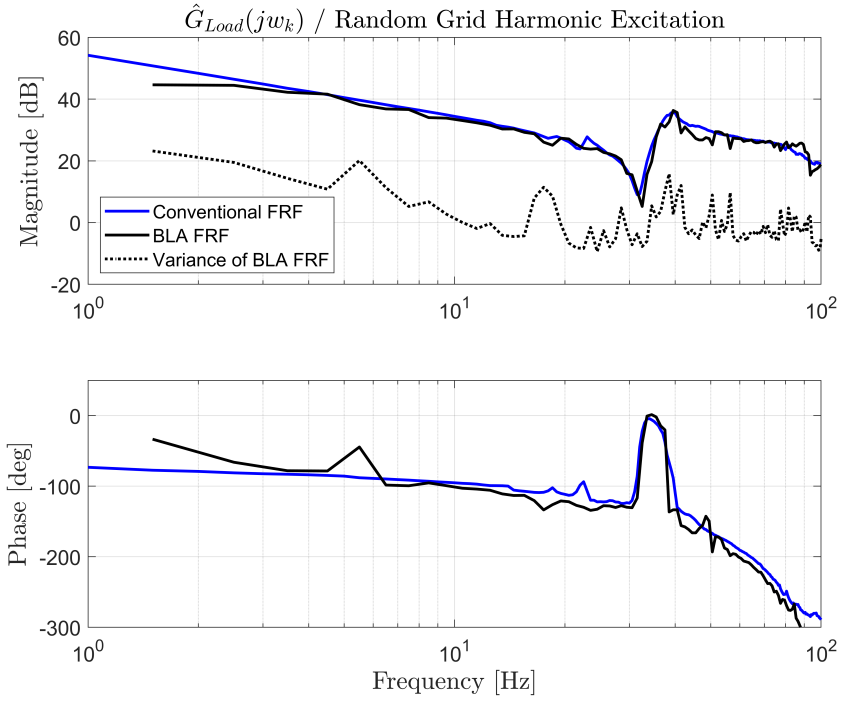

(b)

Figure 3.10: The nonparametric model obtained using BLA from torque input to motor speed output (a), and load speed output (b) with the random grid harmonic random phase multisine excitation.

To complete the identification of the BLA model, the nonparametric model of lowest variance within same measurement period is selected. Chosen model is based on the white noise excitation signal. After this point, standardized loop shaping procedure is applied in order to determine the parameters of PI feedback controller. The command tracking requirements of the system is defined as having a minimum bandwidth of 6 Hz, a gain margin of 3-6 dB, and a phase margin of 30-60 deg. The system with the designed PI feedback controller is considered as a reference point in nonlinear identification and compensation process.

Chapter 4

Nonlinear Identification and Compensation

In order to perform the nonlinear identification, the system behavior is considered as nonlinear, causal and time invariant with an output that contains harmonic spectral components Kw_0 ($K \in \mathbb{N}$) to a sinusoidal input with a frequency w_0. For this case, essential difference of a nonlinear system from a linear counterpart is the harmonic contribution in the response to an sinusoidal input signal with a fundamental frequency w_0. The concept of the optimal compensator is simply based on the minimization of the harmonic components except the fundamental frequency, i.e., $K > 1$. The minimization process make the system as close to a linear system as possible.

To initially highlight the nonlinear dynamics of the system, nonlinear bode plot $\mathfrak{B}(w, \gamma)$ is obtained through NFRF methods excluding phase data. System is considered as uniformly convergent for a bounded continuous input signal of $u(t) = \gamma sin(wt)$ with a frequency w and an amplitude γ. The nonlinear Bode plot of the plant dynamics is obtained and visualized in Fig. 4.1.

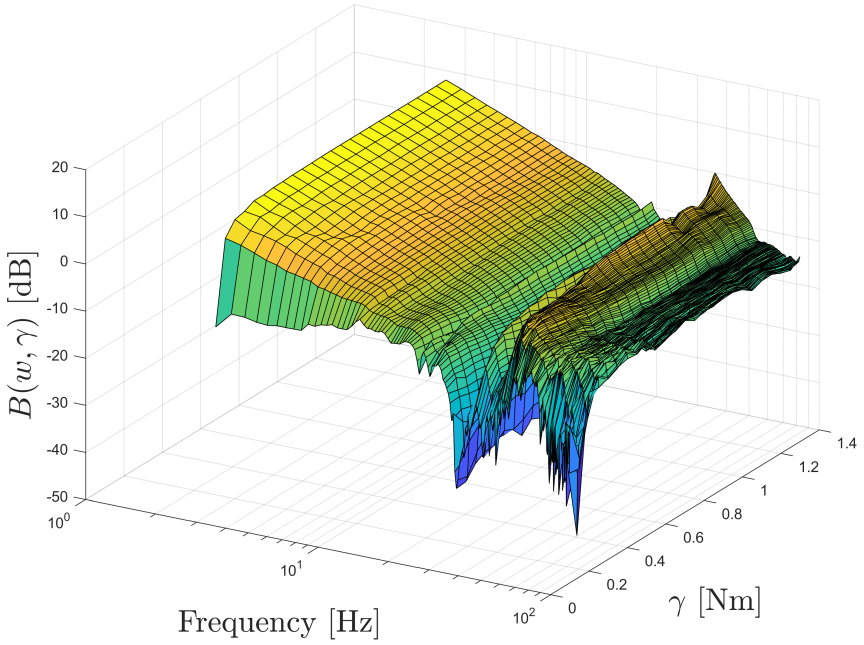

Figure 4.1: Nonlinear Bode plot $\mathfrak{B}(w,\gamma)$ of the experimental setup.

System, subjected to a sinusoidal input $u(t) = \gamma sin(wt)$, is defined in eqn. (4.1).

$$\mathfrak{B}(w,\gamma) = \frac{1}{\gamma}\left(\sup_{t\in\left[\frac{-\pi}{w},\frac{\pi}{w}\right)} |\mathfrak{N}_o(\mathfrak{N}_s(\mathfrak{s},\mathfrak{c},w))|\right), \tag{4.1}$$

where $\mathfrak{s} = \gamma sin(wt)$, $\mathfrak{c} = \gamma cos(wt)$. $\mathfrak{N}_o(.)$ and $\mathfrak{N}_s(.)$ are the corresponding Nonlinear Output Frequency Response Function (NOFRF) and the Nonlinear State Frequency Response Function (NSFRF), respectively [24]. From the nonlinear Bode plot of the plant, resonance and anti-resonance pairs can be observed above 17Hz, which are induced by the driveline stiffness, damping and the inertia J. As it can be seen from low amplitude levels, system behavior suffers from the friction. Based on this nonlinear behavior of the system, it can be concluded that the nonlinear analysis and compensation of the system is crucial to eliminate observed friction based nonlinear behavior.

4.1 Nonlinear Identification using HOSIDF Analysis

Essential information is obtained from the nonlinear Bode plot to define the excitation level and frequency for the HOSIDF measurements. In order to clearly observe the friction based nonlinear region, the input signal is selected at a low frequency and a small amplitude range. System should be excited both below and above the friction dominated stick-slip region using amplitude sweep of excitation. On the other hand, excitation signal should have low frequency in order to distinctly observe friction dominated stick-slip region and have a response in phase with input signal, from the Single-DoF vibration theory [40]. Using low frequency excitation signal also enables to avoid additional nonlinearities due to high frequency components of system behavior. Figure 4.2 shows the input torque signal and the response of the system.

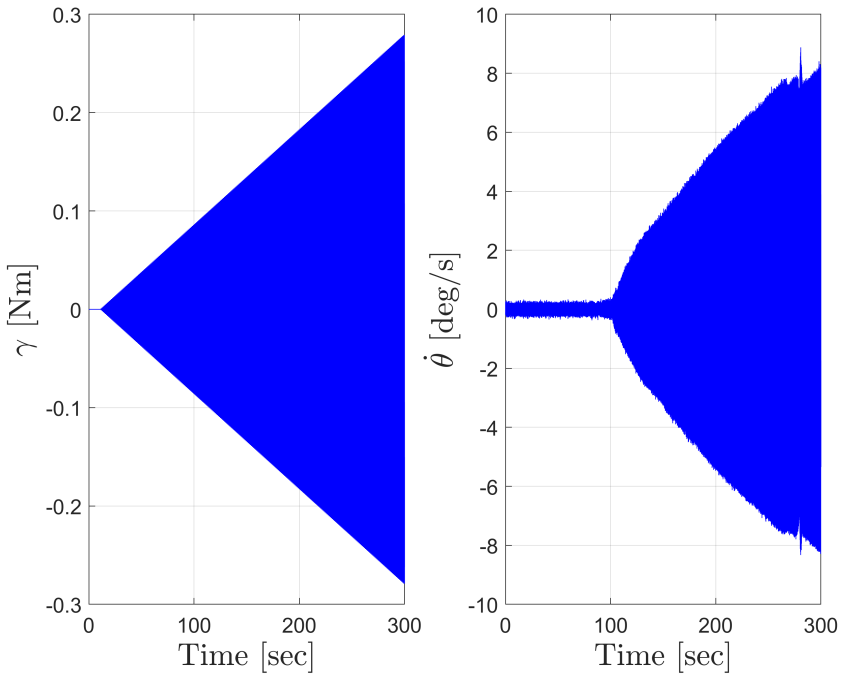

Figure 4.2: Input and output signal example for HOSIDF measurements at 5 Hz.

As presented in Fig. 4.2, the input signal is governed by the information obtained from the nonlinear Bode plot, for the measurement of nonlinear behavior using HOSIDF. The excitation frequency of 5 Hz is selected to guarantee low frequency behavior. Furthermore, input range of amplitude for HOSIDF measurement is considered to be the range that excites the system around its friction dominated stick-slip region. Therefore, amplitude range of 0 to 0.3 Nm are divided into 300 equidistant intervals. For all amplitude levels, system is excited for 5 cycles to eliminate transient effects.

Consider the system is excited using sinusoidal input defined as eqn. (4.2).

$$u(t) = \gamma cos(w_0 t + \varphi_0) \tag{4.2}$$

Corresponding nonlinear harmonic response can be defined as eqn. (4.3):

$$y(t) = \sum_{k=0}^{K} |H_k| \, \gamma^k cos(k((w_0 t + \varphi_0) + \angle H_k), \tag{4.3}$$

along with the k^{th} higher order sinusoidal input describing function $H_k(w_0, \gamma)$ introduced in eqn. (4.4):

$$H_k(w_0, \gamma) = \frac{Y(kw_0)}{U^k(w_0)}, \tag{4.4}$$

where $Y(kw_0)$ is the corresponding higher order response and $U^k(w_0)$ is defined as eqn. (4.5):

$$U^k(w_0) = \prod_{l=1}^{k} U(w_o) \tag{4.5}$$

In Fig. 4.3, the HOSIDF measurements are obtained using Fast Fourier Transform (FFT) method along with the idea of virtual harmonic generator [27]. Each

higher order sinusoidal input describing function is calculated using eqn. (4.3) to eqn. (4.5).

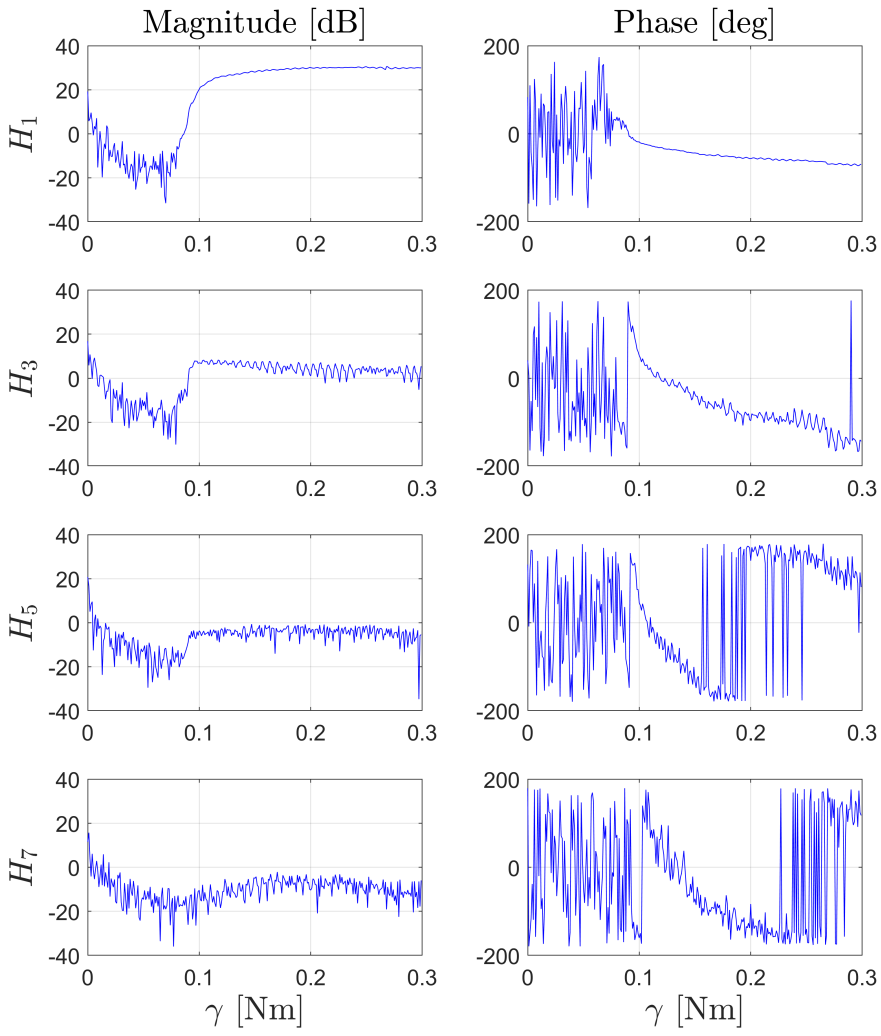

Figure 4.3: HOSIDF measurements of the experimental setup.

From the magnitude plot of first order sinusoidal input describing function, relation of gain with amplitude can be examined. Although from 0.07 Nm to 0.2 Nm, dependency of system gain to excitation amplitude is observable, after 0.2 Nm, system gain is not essentially dependent on the excitation amplitude. However, even after the excitation level of 0.2 Nm, nonlinear behavior can be observed from the magnitude plots of higher order sinusoidal input describing

functions. In higher orders starting from H_3, system gain decreases until a certain level of minimum due to the uncertainties based on low signal-to-noise ratio. After that level, it reaches a certain gain again even for higher harmonics. This gain is related to the contribution from higher order harmonics.

4.2 Compensation of Nonlinear Effects

Based on the amplitude dependency of HOSIDF results given in Fig. 4.3, HOSIDF analysis can be considered as a descriptive tool for the examination of amplitude dependency of the nonlinear systems with harmonic responses. Hence, the HOSIDF technique can be utilized as an optimization tool in order to obtain the optimal feedforward compensation for different feedforward friction compensation techniques as presented in [33] and [34]. In this context, the optimality is the minimization of the difference between the nonlinear system and its linearized counter part. The idea of optimal compensator is simply based on the elimination of the harmonic spectral components Kw_0 ($K \in \mathbb{N}$) except the fundamental frequency, i.e., $K > 1$, to sinusoidal input with frequency w_0.

Among other nonlinear behaviors, characteristic behavior of friction has a great influence on the performance and precision of the motion platform. Different friction models [41] can be implemented as a model for feedforward compensation [42, 43, 44]. The experimental setup is utilized in order to identify the required optimal feedforward gain. Even though the pure Coulomb friction feedforward design improves the system performance as implemented in [33], discontinuous characteristics of the model is not well-suited for all dynamic systems. More complex friction models like LuGre model is introduced in feedforward methods [34] and adaptive techniques are studied as compensation tools [45, 46, 47]; however, complex friction models are highly dependent on the parametric changes on the system due to manufacturing processes or environmental conditions. Therefore, Stribeck friction model given in eqn. (4.6) is selected as a base point in order to obtain a continuous and neat feedforward signal compared to Coulomb and LuGre friction models. The Stribeck friction model describes the friction torque

in a rotational system as:

$$T_f = \begin{cases} s(w) + \sigma_2 w & \text{if } w \neq 0, \\ T_a & \text{if } w = 0 \text{ and } |T_a| < T_s, \\ T_s * \text{sgn}(T_a) & \text{otherwise.} \end{cases} \tag{4.6}$$

In this context, w is the angular velocity, T_f, T_a and T_s are the friction, applied input and stiction torques, respectively, and σ_2 is the viscous term. Stribeck exponential curve $s(w)$ in eqn. (4.6) is defined as:

$$s(w) = (T_c + (T_s - T_c)e^{\left|\frac{w}{w_s}\right|^{\delta}}) * \text{sgn}(w), \tag{4.7}$$

where T_c, w_s and δ are the Coulomb torque, Stribeck velocity and Stribeck exponent, respectively.

The parameters of the Stribeck model are identified using the Nelder-Mead optimization algorithm. The special excitation signal is generated from a band limited random signal up to 4 Hz, enveloped by the sum of first three non-zero terms of Fourier series of the rectangular signal [35]. This speed reference enables the system to cross zero velocity line with different amplitudes and frequencies within a short time period. The excitation signal used as a speed reference is given in Fig. 4.4a and identified Stribeck model is illustrated in Fig. 4.4b. The parameters of the model are given in Table 4.1.

Table 4.1: Stribeck Model Parameters

Parameter	**Identified Value**
Stiction Torque (Nm)	$T_s = 0.3160$
Coulomb Torque (Nm)	$T_c = 0.2432$
Stribeck Velocity (rad/s)	$w_s = 0.0247$
Stribeck Exponent	$\delta = 1$

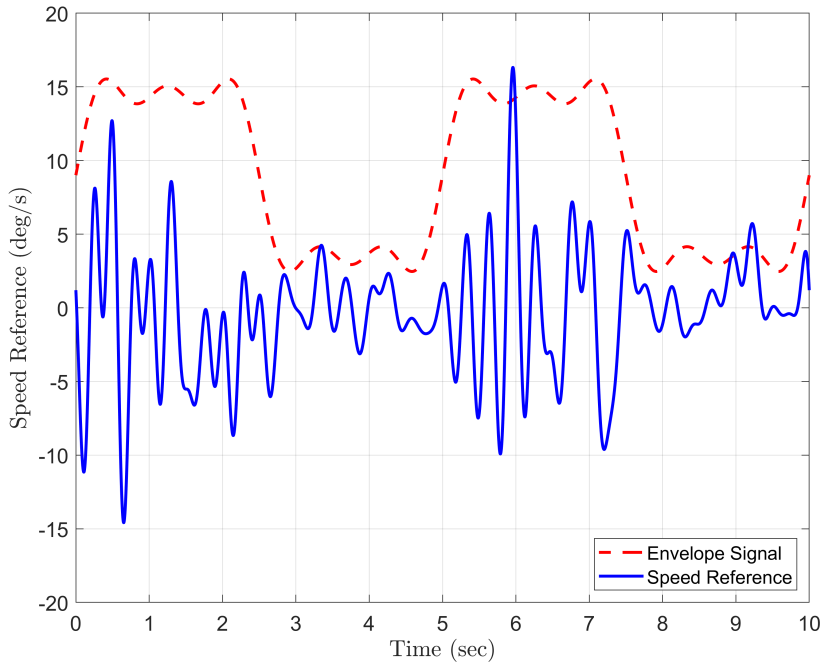

(a)

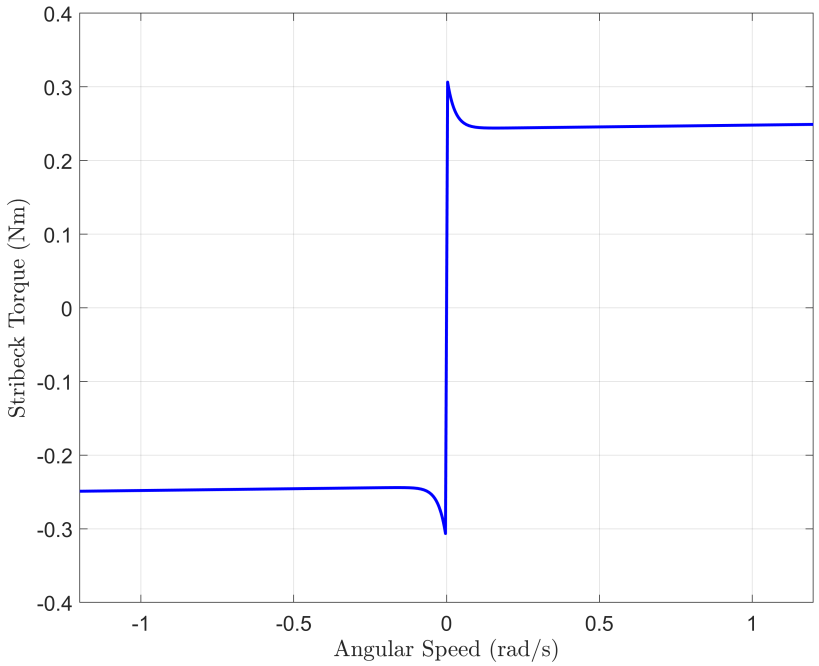

(b)

Figure 4.4: The speed reference signal for the Stribeck model identification process (a), and identified Stribeck model (b).

After the identification, instead of using the friction model output directly, it is normalized to the interval of $[-1, 1]$ at low velocity interval by dividing the output by T_s and a gain of K is utilized in order to determine final feedforward signal. The block diagram of the overall compensation strategy is given in Fig. 4.5.

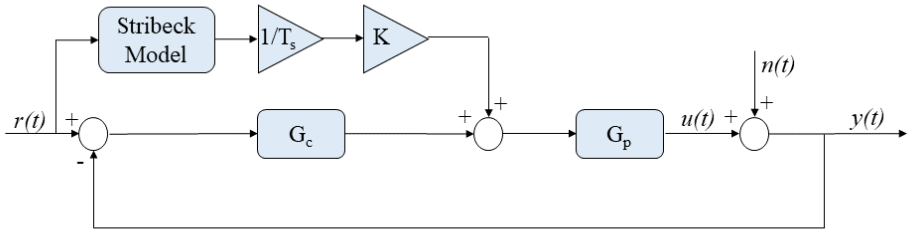

Figure 4.5: The block diagram of nonlinear compensation strategy.

As it can be seen from the block diagram given in Fig. 4.5, experimental setup is initially subjected to a PI feedback controller in order to satisfy system requirements mentioned previously. Upon this strategy, feedforward compensation is applied to the system with an increasing K value in order to understand the effect of feedforward gain to harmonic response measurements.

To define the optimal case, the concepts of linear and nonlinear systems are compared. As a final goal, a nonlinear system is subjected to feedforward compensator in order to approximate a linear system as much as possible. The key difference of nonlinear system and linear system is the higher order harmonics observed in nonlinear behavior. In a linear system, response to a fundamental frequency input is only a fundamental frequency output. On the other hand, response to a fundamental frequeny input may consist of higher order harmonic components in a nonlinear system. In order to obtain closest form of nonlinear system to linear system, higher order harmonics in the response to a fundamental frequency should be minimized. Therefore, feedforward gain can be stated as optimal where the response of the system has minimum proportion of the sum of all harmonics contribution to the magnitude of fundamental frequency contribution.

Optimal gain for feedforward compensation FF_{Kopt} is obtained using cost function as:

$$FF_{Kopt} = \arg \min_{FF_K \in \mathbb{R} \geq 0} \frac{1}{N_{\mathbb{K}}} \frac{\sum_{k \in \mathbb{K}} |\mathbb{E}\{Y(kw_0)\}|}{|\mathbb{E}\{Y(w_0)\}|}, \tag{4.8}$$

where $\mathbb{K}\{k \in \mathbb{N} \geq 2 | \mathbb{E}\{Y(kw_0)\} \neq 0\}$ with $\eta-$confidence level as initially introduced in [33]. This cost function, when minimized, guarantees that the feedforward constant K found will maximize the relative magnitude of the fundamental frequency and make the system behave as linear as possible.

So, the noise in the experimental data should be considered and only the harmonics with a high signal to noise ration should be taken into account [34]. Only the harmonics with $\eta-$confidence level are taken into account in the HOSIDF process. Harmonics without $\eta-$confidence level are ignored, since the noise level of those harmonics are higher than the harmonic signal. This property can be considered as the quality assessment of the measurements on harmonics. The expected value of the sample mean $|\mathbb{E}\{Y(w_0)\}|$ is not equal to 0 with at least $\eta-$confidence level if the criterion given in eqn. (4.9) is greater than the corresponding cumulative distribution function.

$$\frac{\left|\bar{Y}(kw_0)\right|^2}{\sigma_y^2(kw_0)} > F^{\eta}_{2,2(N-1)}, \tag{4.9}$$

where $F^{\eta}_{2,2(N-1)}$ is defined as the cumulative $F_{2,2(N-1)}$ distribution cdf($F^{\eta}_{2,2(N-1)}$) $= \eta$ [33].The sample mean and variance on sample mean are defined as equations (4.10) and (4.11), respectively.

$$\bar{Y}(kw_0) = \frac{1}{N} \sum_{n=1}^{N} Y_n(kw_0) \tag{4.10}$$

$$\sigma_y^2(kw_0) = \frac{1}{N(N-1)} \sum_{n=1}^{N} (Y_n(kw_0) - \bar{Y}(kw_0))^2 \tag{4.11}$$

The optimal feedforward gain is achieved using K values in the range of [0,0.14] with 50 equal intervals until overcompensating the setup, i.e., observing exceeding velocity feedback with respect to reference velocity during direction changes. In the experiment, a sinusoidal speed reference of $\gamma = 2$ and $w_0 = 0.5$ is used as the excitation signal.

Using the experimental data, the input and the output spectra are calculated using FFT. Then, output spectrum of the system is evaluated using equations (4.8) and (4.9). Only the harmonics that satisfy the confidence level criterion given in eqn. (4.9) are used in the calculation of the optimal feedforward gain. The harmonic responses and the confidence level criterion of the scenario without feedforward is given along with chosen harmonics in Fig. 4.6a. Using only the chosen harmonics satisfy the measurement quality of the methodology. $\eta-$ confidence level is defined for only the harmonics greater and equal to 2 in order to use these harmonics in the calculation of the optimal feedforward gain.

The optimal feedforward gain is calculated using only the related response harmonics and eqn. (4.8), as shown in Fig. 4.7a. Once the feedforward gain is increased with a relevant step, the magnitude in corresponding harmonics are decreased proportionally to the excitation frequency. As it can be seen from Fig. 4.7a, the feedforward gain of K = 0.0808 minimizes the optimal feedforward gain criterion in eqn. (4.8). As the corresponding HOSIDF is considered, the optimal feedforward gain can be also verified in the odd harmonic responses of the system due to odd nonlinear characteristics. The decrease in the contribution of the normalized odd higher order harmonics can be observed from Fig. 4.7b.

For the desired compensation, the selection of K = 0.0808 can be considered as the optimal feedforward gain. The harmonic responses and the confidence level criterion of the optimal gain is given in Fig. 4.6b. Similarly, same harmonics selected for without feedforward case are highlighted for the optimal feedforward case. As it can be seen from the magnitude graphs of relevant harmonics, all higher order harmonics decreased in contrast of fundamental harmonic frequency. The optimal case stands for the scenario where the effects of higher harmonics are minimum compared to the fundamental harmonic frequency.

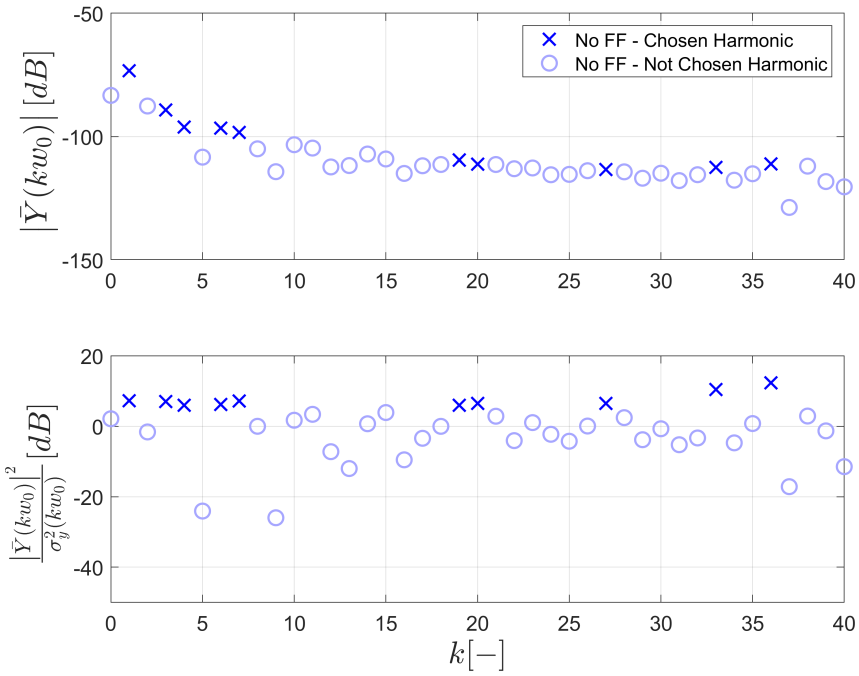

(a)

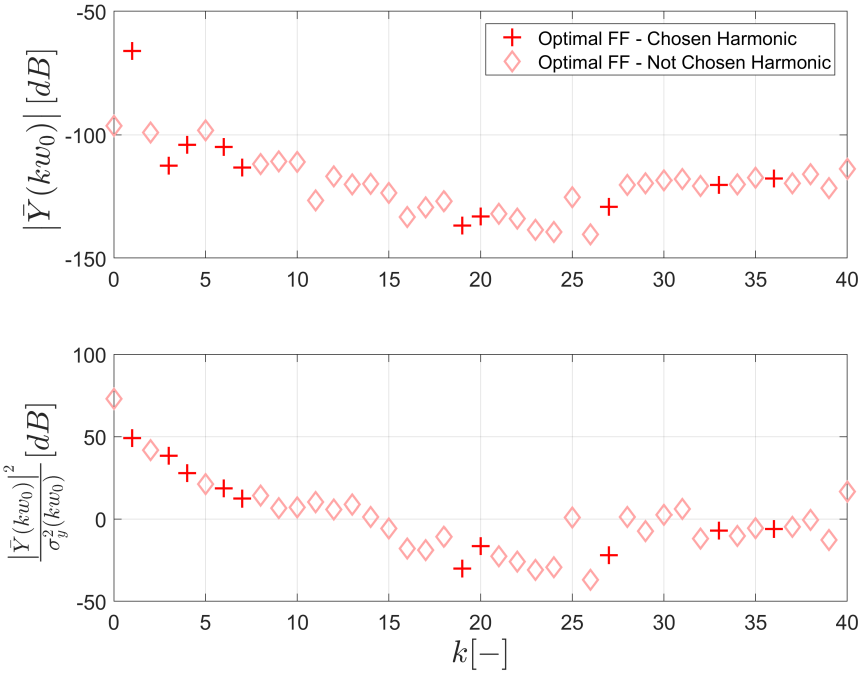

(b)

Figure 4.6: Harmonic responses and the confidence level of the harmonics without the feedforward compensation (a), and with the optimal feedforward compensation (b).

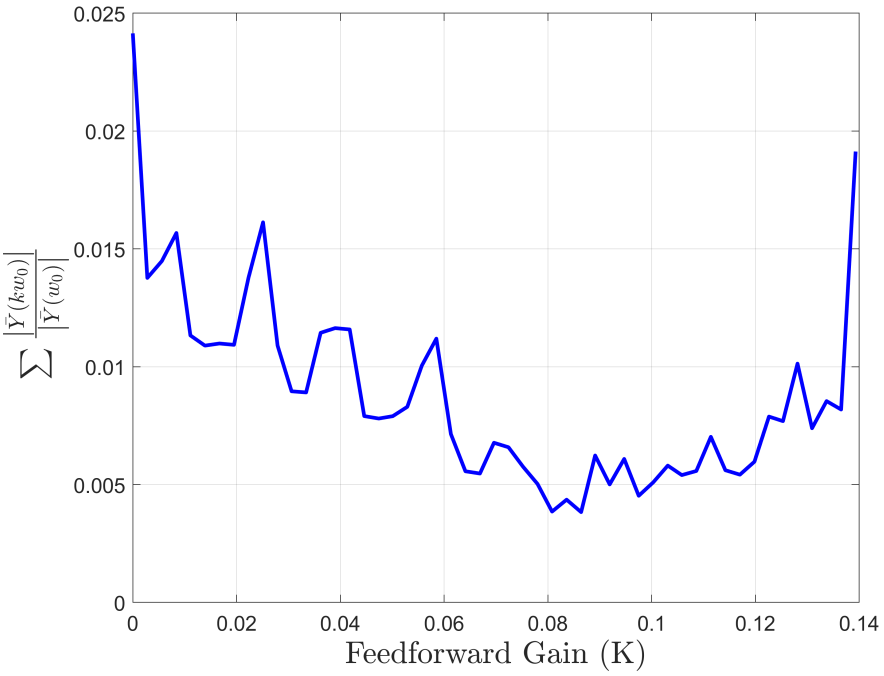

(a)

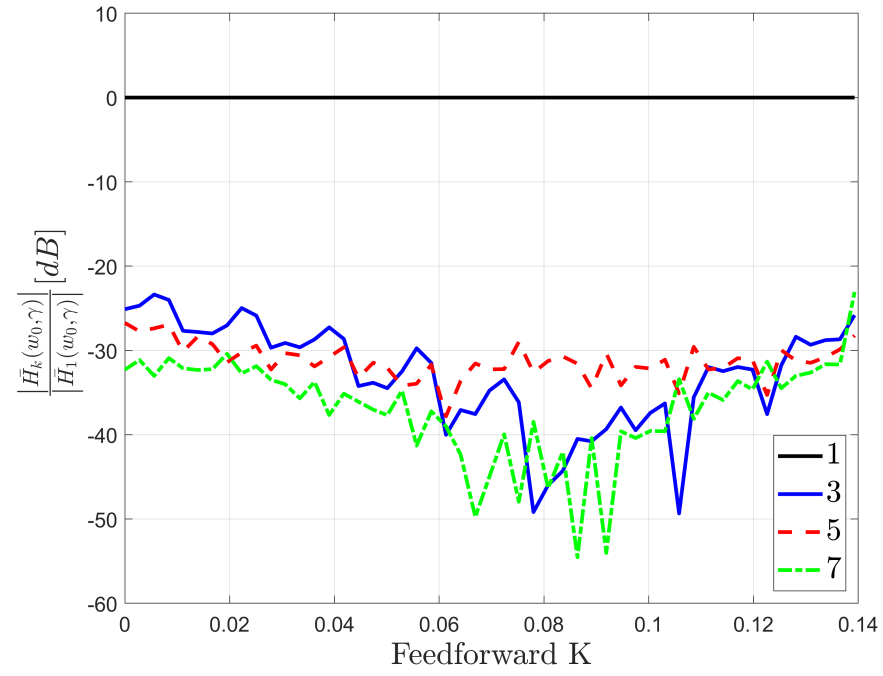

(b)

Figure 4.7: The optimal feedforward compensation gain criterion evaluated at different gains (a), and the normalized odd harmonics of HOSIDF measurements changing with feedforward gain (b).

To observe the magnitude decrease in the relevant harmonics for optimal feedforward compensation, $\left|\bar{Y}(kw_0)\right|$ values are shown in Fig. 4.8. By only applying the optimal feedforward compensation with the classical PI feedback controller, significant decrease in $\left|\bar{Y}(kw_0)\right|$ for higher order harmonics can be observed. For instance, third and seventh harmonics decreased around 22 and 14 dB, respectively. In contrast, the $\left|\bar{Y}(kw_0)\right|$ for the fundamental frequency is increased almost 10 dB for the optimal feedforward compensation. The increase in the contribution of fundamental frequency is a mathematical side effect of the feedforward compensation [34]. In the optimal case, the response of the system includes almost the same fundamental response. However, higher harmonics in the response are dramatically decreased, leading to an increase in the fundamental frequency contribution.

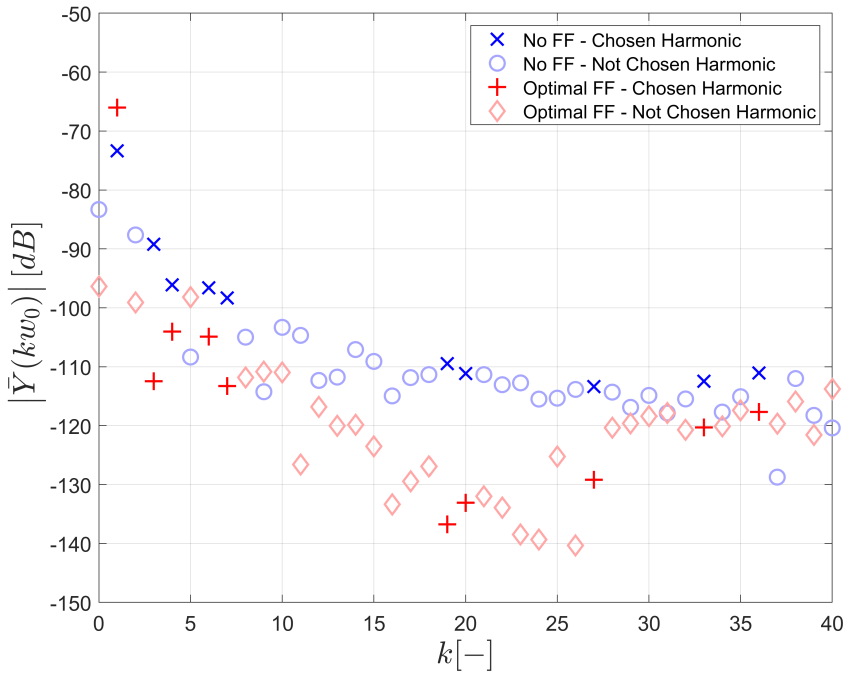

Figure 4.8: Magnitude difference in the relevant harmonic responses in optimal feedforward compensation.

Chapter 5

Results and Discussion

After the nonlinear identification and the feedforward optimization process, system is subjected to a reference tracking scenario in order to evaluate the performance of the presented process. In this context, a benchmark sinusoidal reference tracking input signal is applied to the system for both cases of without feedforward case and the optimal feedforward case. To demonstrate the performance of the procedure, methodology is applied not only to the experimental setup, but also to RCWS, Remote Controlled Weapon System which have different system characteristics of inertia, friction and backlash. By this way, methodology is tested under various dynamic systems.

5.1 Results for Experimental Setup

Performance measurements are conducted with the reference sinusoidal speed input signal with $\gamma = 2$ and $w_0 = 0.5$, as in the identification phase. Then, reference tracking performance results are obtained for without feedforward compensation and with the optimal feedforward compensation using K = 0.0808. For both cases, same LTI PI feedback controller mentioned previously is used. The sinusoidal reference tracking of the system is given in Fig. 5.1a and Fig. 5.1b.

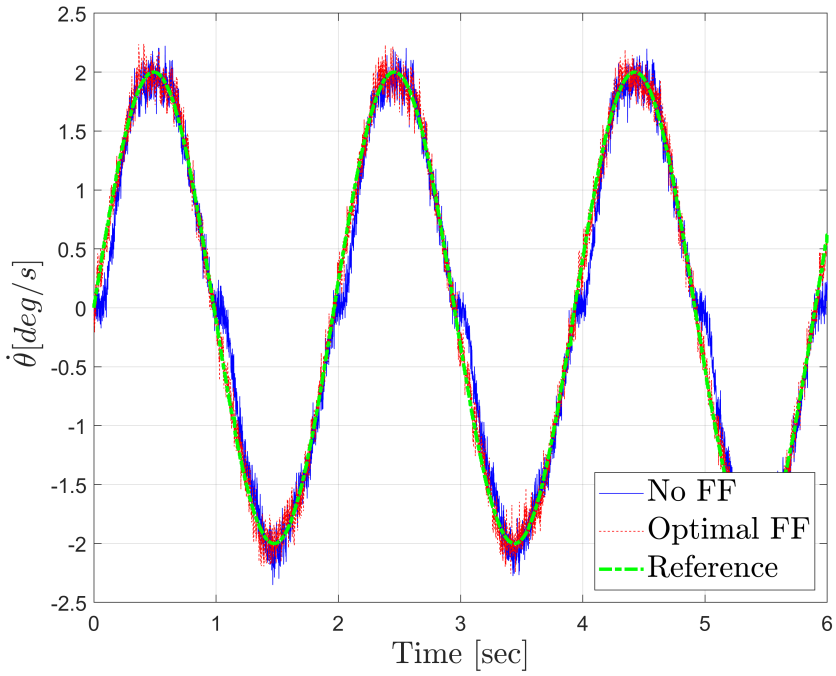

(a)

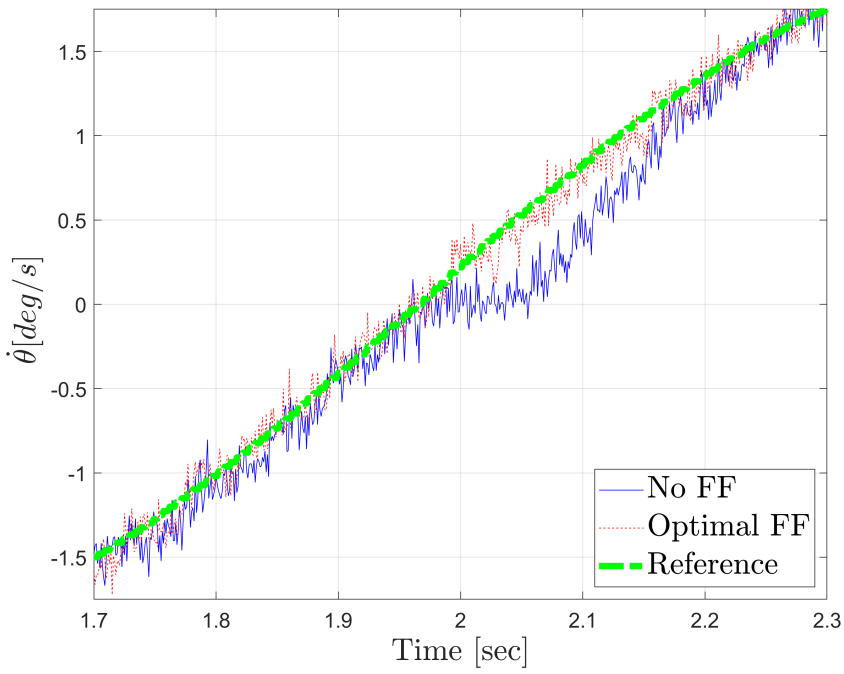

(b)

Figure 5.1: Sinusoidal reference signal tracking without feedforward compensation and with the optimal feedforward compensation (a), and zero reference crossing in closer view (b).

The results show that, the optimal feedforward compensation enables the system to achieve better reference tracking for zero crossing reference changes, which is the region where friction and backlash effects are most dominant. To quantify the performance for both cases, RMS tracking error is used, which is given in eqn. (5.1):

$$E_{RMS} = \sqrt{\frac{1}{M}\sum_{m=1}^{M}(u_m(t) - y_m(t))^2} \tag{5.1}$$

For the measurement given in Fig. 5.1a, the average RMS tracking errors without feedforward compensation and with the optimal feedforward compensation are 0.0431 deg/s and 0.0117 deg/s, respectively. This difference in errors is mainly originated from the nonlinearities of the system and the performance of the introduced feedforward compensation. The reference tracking error of same measurement is illustrated in Fig. 5.2.

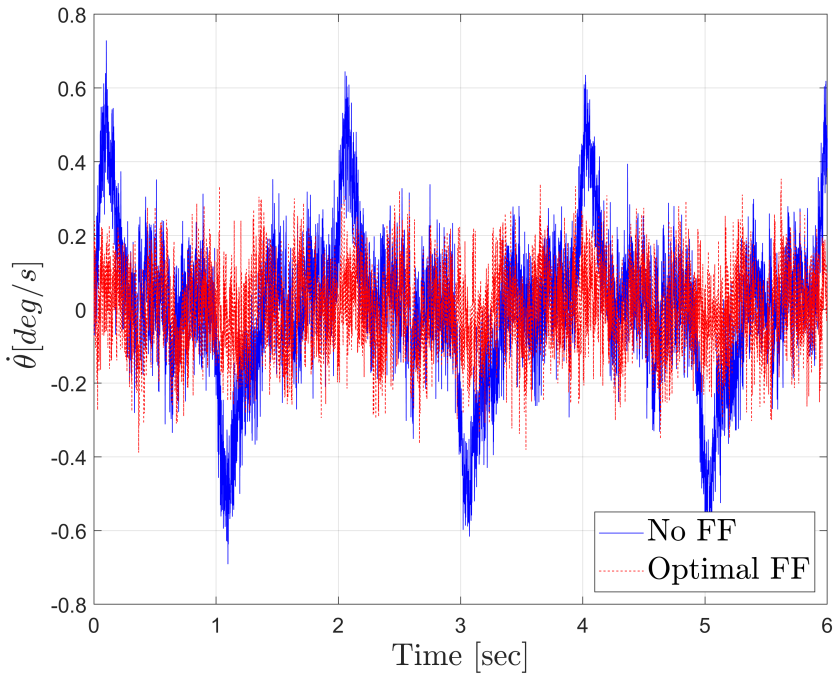

Figure 5.2: The error plot of reference signal tracking without feedforward compensation and the optimal feedforward compensation.

Fig. 5.2 states that the optimal feedforward strategy eliminates the error peaks around zero crossings. To quantify the performance benefit of the methodology in depth, error data is integrated and polynomial trend over the integrated data is removed to calculate the standard deviation over the integral of error.

For the given error integral in Fig. 5.3, corresponding standard deviations without feedforward compensation and with the optimal feedforward compensation are 0.0382 deg and 0.0051 deg, respectively.

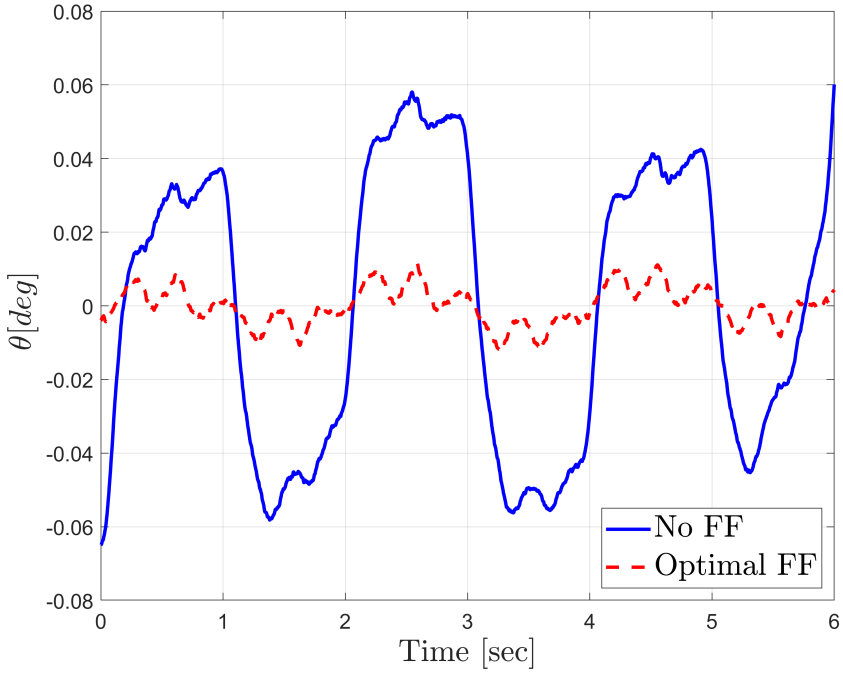

Figure 5.3: Error integral plot of reference signal tracking with no feedforward and optimal feedforward compensation.

In order to present a summarized performance quantification of the feedforward methodology, all results are presented in Table 5.1. It is seen from the Table 5.1 that, utilization of the optimal feedforward compensation improves the reference tracking performance dramatically. This behavior have great influence on the systems which work under low speed reference tracking requirements with zero crossings.

Table 5.1: Performance Measures for Experimental Setup

Scenario	Without FF	With the Optimal FF
RMS Tracking Error (deg/s)	0.0431	0.0117
STD of Error Integral (deg)	0.0382	0.0051

Fig. 5.4 illustrates the torque input generated by the controller. Only the PI feedback controller generates torque in the case without feedforward compensation. Significant difference in zero crossing can also be observed from the torque data.

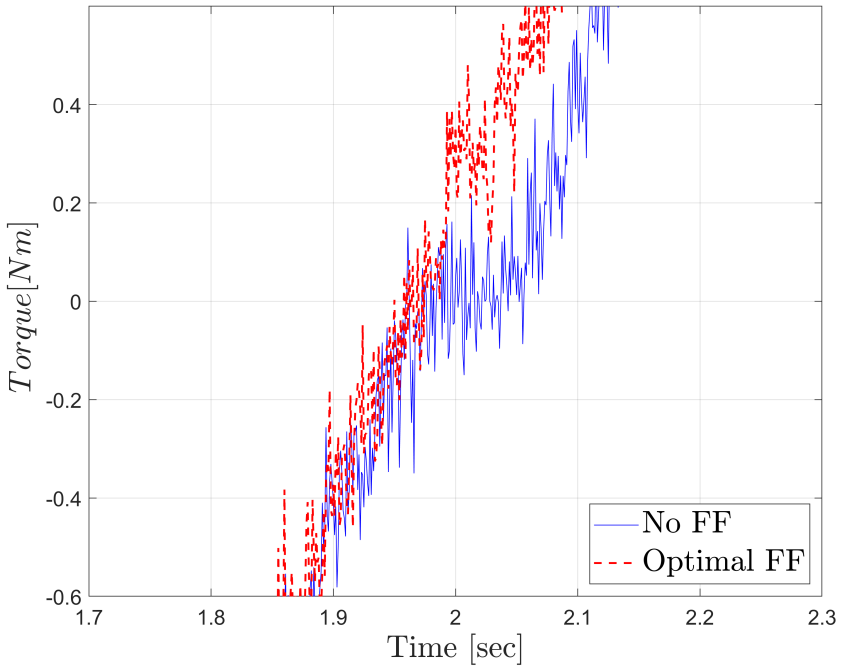

Figure 5.4: Torque difference in zero crossing during sinusoidal reference signal tracking with no feedforward and optimal feedforward compensation.

5.2 Results for RCWS

Presented optimal feedforward procedure is applied to RCWS, Remote Controlled Weapon System presented in Fig. 5.5 [48].

Figure 5.5: RCWS, a Remote Controlled Weapon System

As a standardized procedure, Best Linear Approximation of the system is obtained using white noise excitation signal. Nonparametric models for the motor and the load speed output signals are presented in Fig. 5.6a and 5.6b, respectively.

Measurements are conducted for the reference sinusoidal speed input signal with $\gamma = 2$ and $w_0 = 0.5$, for the aximuth axis of the system similar to the experimental setup. HOSIDF analysis of the RCWS for without feedforward compensation case and the optimal feedforward compensation are illustrated in Fig. 5.7a and 5.7b, respectively. Energy decrease in related HOSIDF for optimal compensation and the selection of optimal feedforward gain is presented in Fig. 5.8a and 5.8b, respectively. Using different measurements and averaging can eliminate the noisy behavior over the curve in 5.8b.

Then, results are obtained for the case without feedforward compensation and with the optimal feedforward compensation using K = 0.1044 Nm. Using the defined optimal feedforward compensation, sinusoidal reference tracking performance of the system is given in Fig. 5.9a and Fig. 5.9b. RMS speed reference tracking errors are 0.0833 deg/s and 0.0256 deg/s for no feedforward and optimal feedforward scenarios, respectively. Fig. 5.10a and Fig. 5.10b shows the speed tracking error and integral of error without polynomial trend similar to the experimental setup.

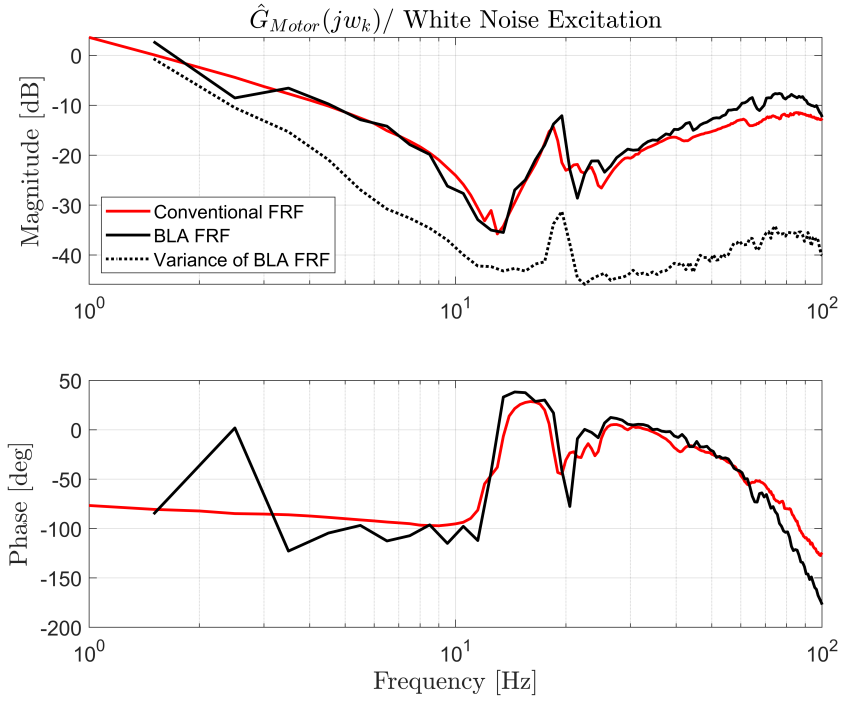

(a)

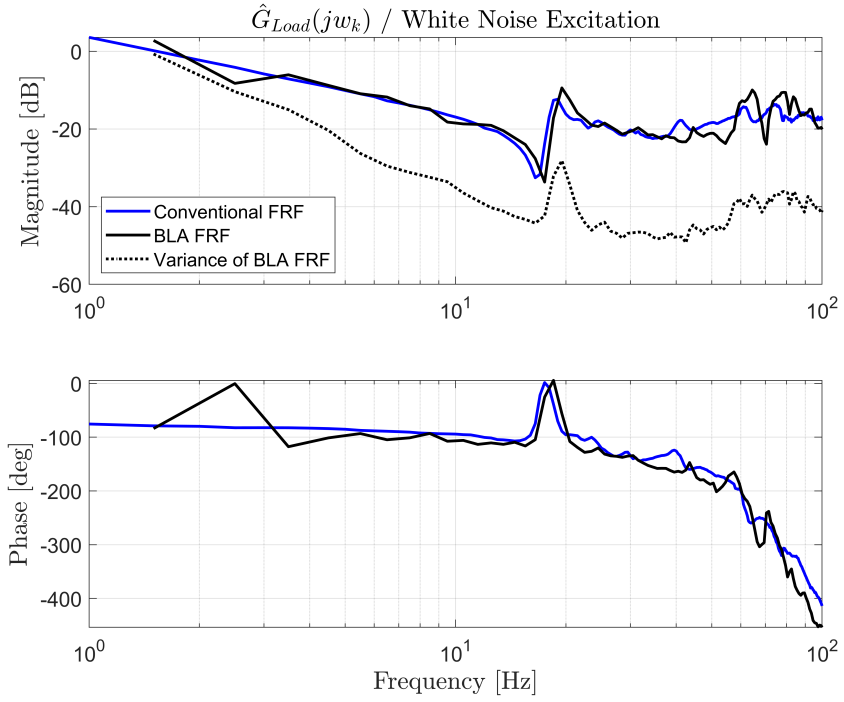

(b)

Figure 5.6: Best Linear Approximation of the RCWS azimuth axis with white noise excitation signal for the motor speed output signal (a), and the load speed output signal (b).

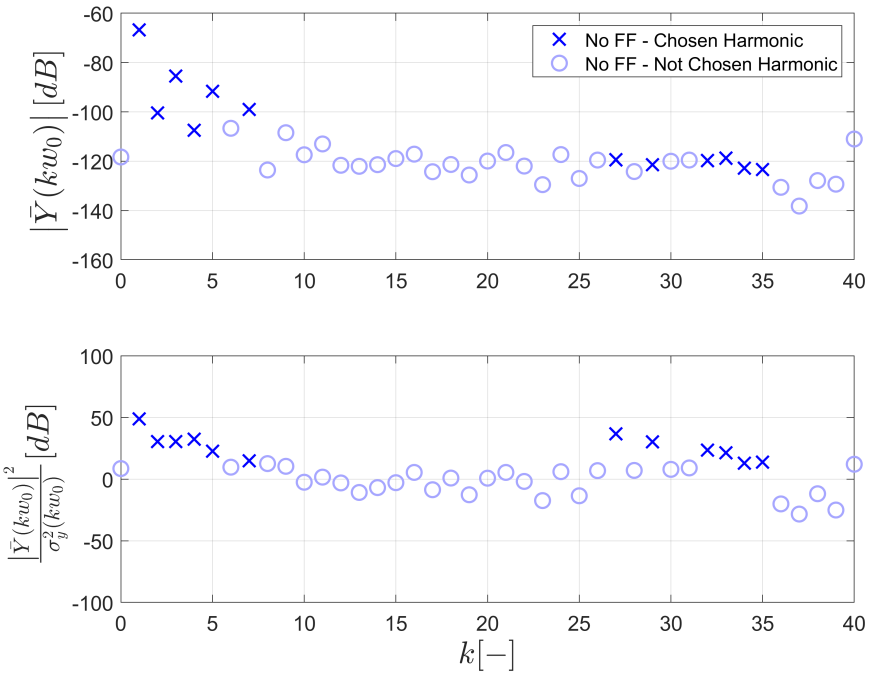

(a)

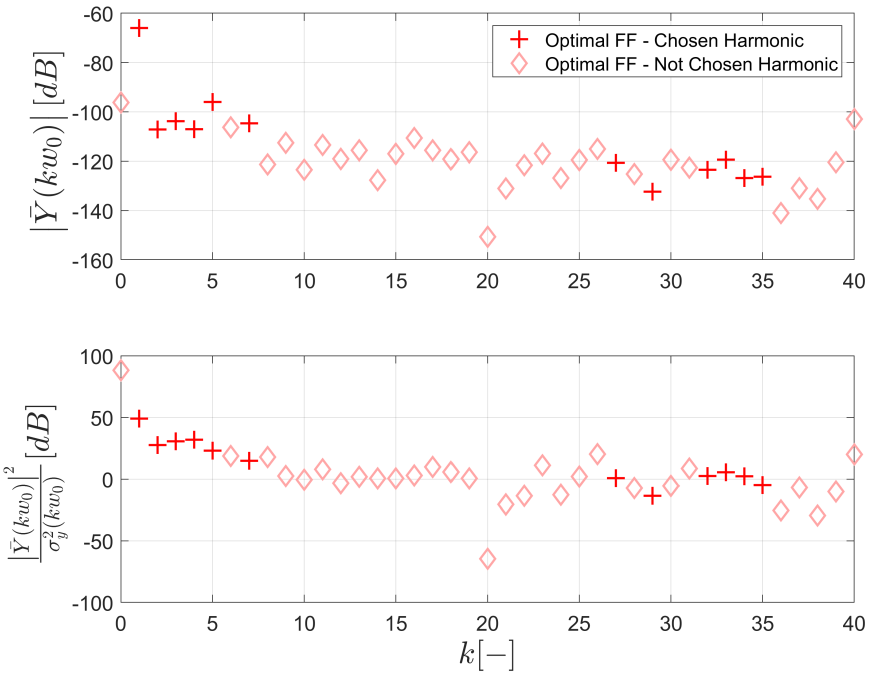

(b)

Figure 5.7: The HOSIDF analysis of RCWS for without feedforward compensation (a) and with the optimal feedforward compensation (b).

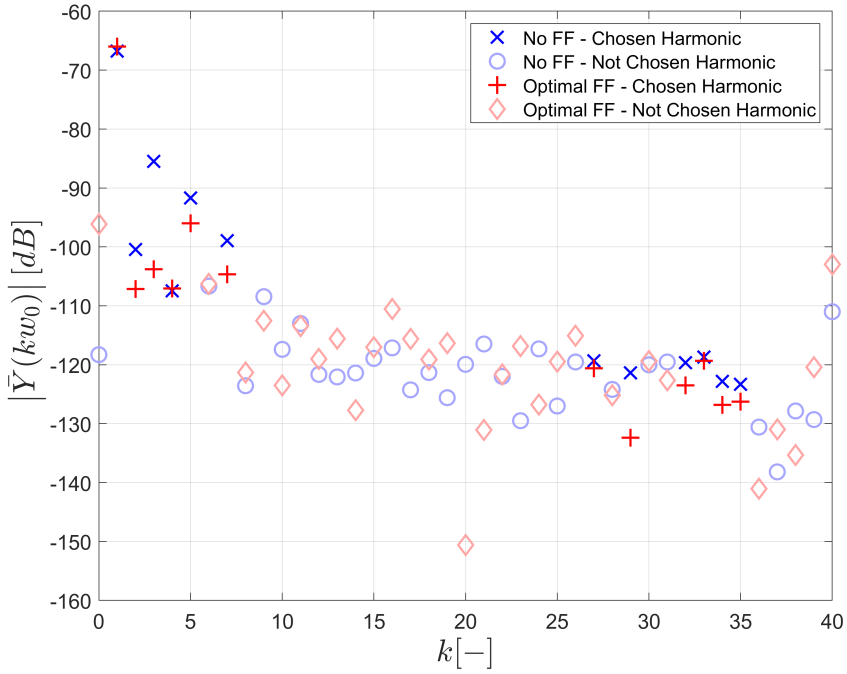

(a)

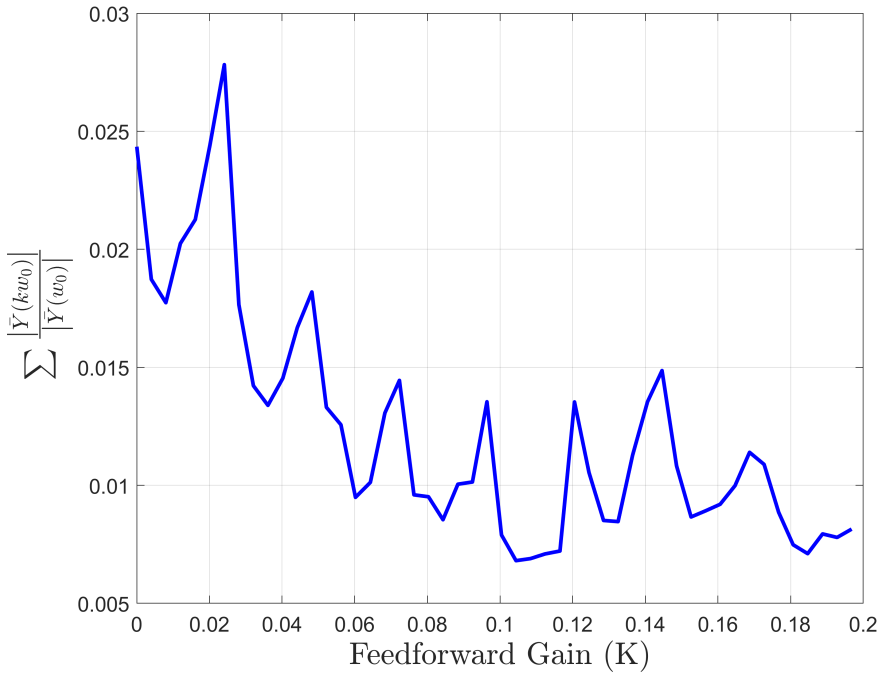

(b)

Figure 5.8: Energy decrease in the HOSIDF analysis of RCWS for without feedforward compensation and with the optimal feedforward compensation (a), and the optimal feedforward compensation gain criterion for different gains (b).

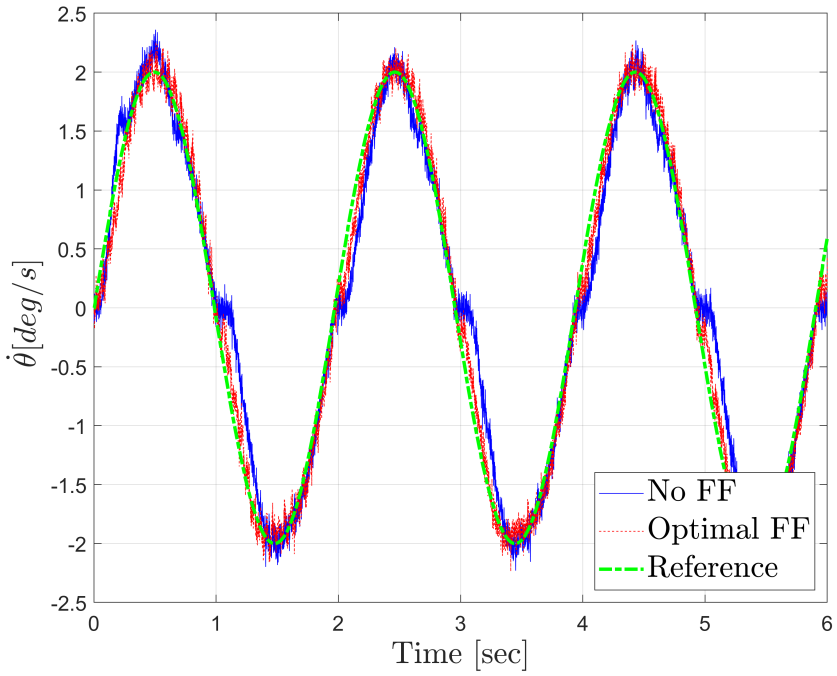

(a)

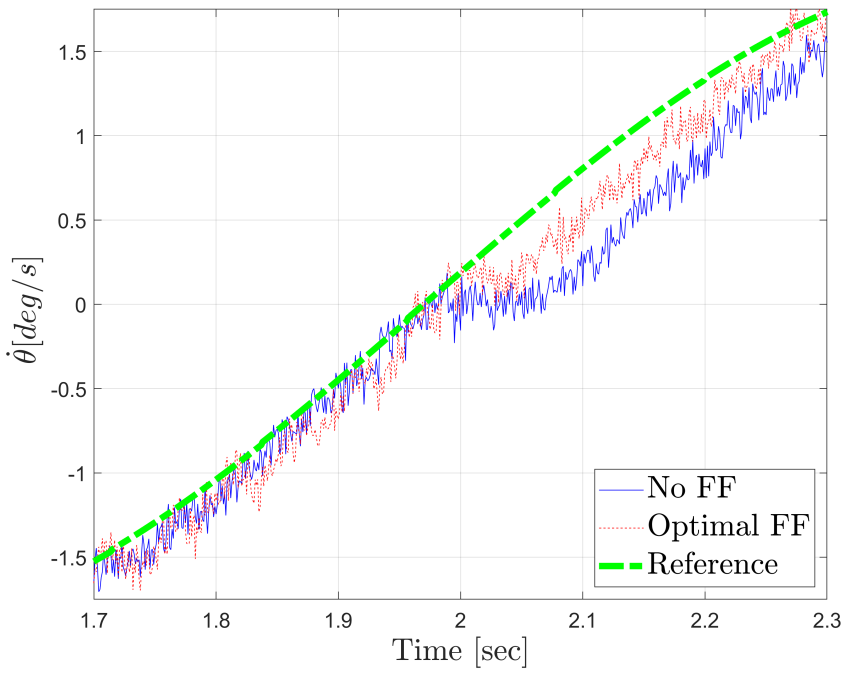

(b)

Figure 5.9: Sinusoidal reference signal tracking for RCWS with no feedforward and optimal feedforward compensation (a), and zero reference crossing in closer view (b).

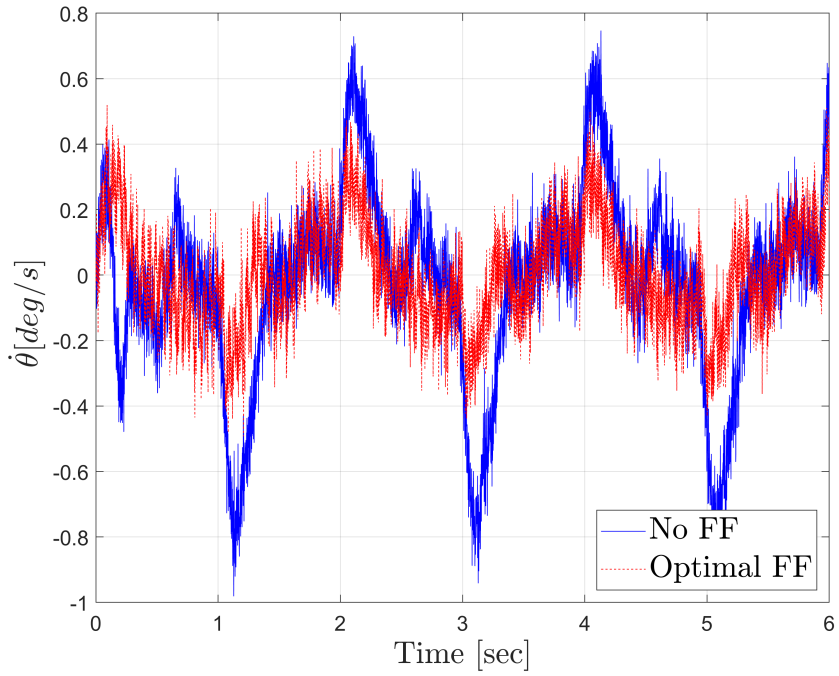

(a)

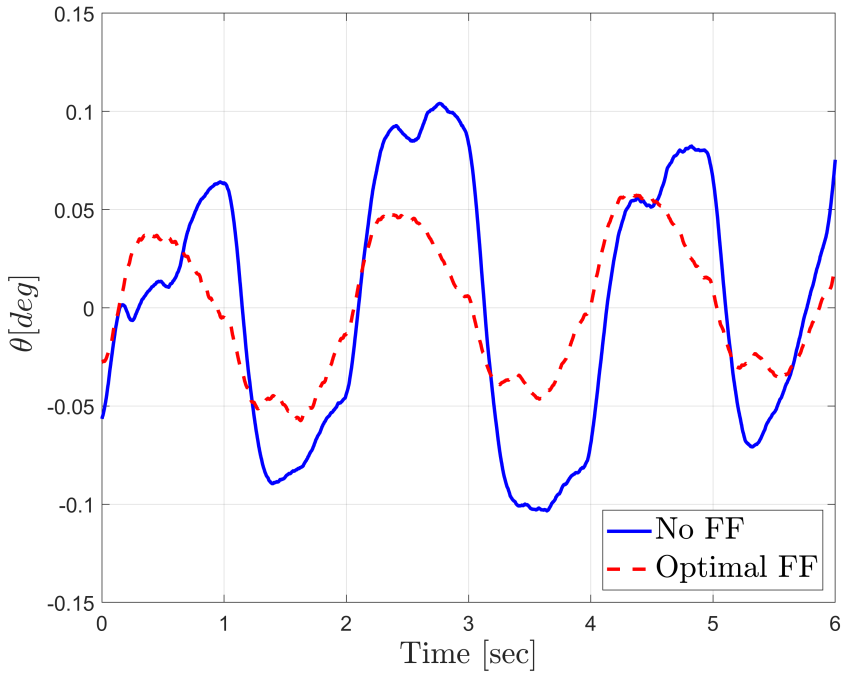

(b)

Figure 5.10: Error (a) and error integral (b) plot of reference signal tracking for RCWS with no feedforward and optimal feedforward compensation.

Standard deviations for no feedforward and optimal feedforward compensations are 0.0653 deg and 0.0341 deg, respectively. To present a summarized performance quantification of the feedforward methodology for RCWS, all results are presented in Table 5.2 similar to the experimental setup.

Table 5.2: Performance Measures for RCWS

Scenario	**Without FF**	**With the Optimal FF**
RMS Tracking Error (deg/s)	0.0833	0.0256
STD of Error Integral (deg)	0.0653	0.0341

As in the case of experimental setup, the optimal feedforward compensation enables the system to perform better reference tracking. Although the kinematic coupling effect can have a influence on the performance for two-axis platforms, dominant friction effects in stick-slip region can be reduced dramatically for azimuth and elevation axis drivelines separately.

Chapter 6

Conclusion

This study presents a standardized method for nonlinear identification and the optimal feedforward friction compensation for a single DoF industrial motion platform. The contribution of this work is to utilize FFT and HOSIDF based frequency domain identification techniques from the literature in the optimization of feedforward friction compensation design with the Stribeck friction model. The design presents a comprehensive feedforward method for the optimal nonlinear friction compensation for dynamic systems with harmonic responses. The model is normalized and utilized for feedforward compensation with an optimal gain. The results of the experimental study demonstrate improved system performance and precision in reference tracking.

- A class of time invariant nonlinear systems containing harmonic response to a sinusoidal excitation is subjected to the standardized method for the nonlinear identification and the optimal feedforward compensation of friction characteristics for this work.
- BLA methodology is used to minimize the nonlinear components in the nonparametric model of the system. A classical PI controller is implemented using loop shaping techniqıes so that system meets the linear system requirements.

- Procedure is based on the friction compensation in a single degree of freedom industrial motion platform's driveline, where it is not only valid for specific type of nonlinearity. There exist optimal feedforward friction compensation studies in literature with different friction models. For this work, continuous Stribeck friction model is utilized in order to reduce model complexity while having continuous characteristics. A special reference signal and the Nelder-Mead optimization algorithm are used for the friction model identification process.

- The HOSIDF based optimal feedforward compensation methodology is standardized for a mechatronic application. The optimal compensation is obtained by the minimization of the contributions of higher order ($K > 1$) harmonic components Kw_0 ($K \in \mathbb{N}$) to the output for a sinusoidal input with frequency w_0.

The identification of the plant dynamics and the design of LTI PI controller can be considered as the limitation of the methodology described in this study. Using different identification techniques to obtain high fidelity system models and higher performance feedback controller would improve the performance of the overall methodology. However, the identification and feedback controller design methodology described in this study is suffcient to demonstrate the optimality of the feedforward compensator for described system.

Further research can be directed to the identification of relevant harmonics of HOSIDF method with real-time data. Although the proposed procedure of identification and optimal feedforward gain determination is a straightforward method, online techniques will enable optimal feedforward compensation to be resistant to changes in the system due to manufacturing processes or environmental conditions by motion platform's very nature.

Bibliography

[1] K. J. Åström and P. Eykhoff, "System identification—a survey," *Automatica*, vol. 7, no. 2, pp. 123–162, 1971.

[2] T. Söderström and P. Stoica, *System identification*. Prentice-Hall, Inc., 1988.

[3] R. Johansson, *System modeling and identification*, vol. 1. Prentice Hall Englewood Cliffs, NJ, 1993.

[4] L. Ljung, "System identification," *Wiley Encyclopedia of Electrical and Electronics Engineering*, 2001.

[5] R. Pintelon and J. Schoukens, *System identification: a frequency domain approach*. John Wiley & Sons, 2012.

[6] G. Kerschen, K. Worden, A. F. Vakakis, and J.-C. Golinval, "Past, present and future of nonlinear system identification in structural dynamics," *Mechanical systems and signal processing*, vol. 20, no. 3, pp. 505–592, 2006.

[7] D. Rijlaarsdam, P. Nuij, J. Schoukens, and M. Steinbuch, "A comparative overview of frequency domain methods for nonlinear systems," *Mechatronics*, vol. 42, pp. 11–24, 2017.

[8] M. Schetzen, "The volterra and wiener theories of nonlinear systems," 1980.

[9] L. O. Chua and C.-Y. Ng, "Frequency domain analysis of nonlinear systems: general theory," *IEE Journal on Electronic Circuits and Systems*, vol. 3, no. 4, pp. 165–185, 1979.

[10] X. Jing and Z. Lang, "Frequency domain analysis and design of nonlinear systems based on volterra series expansion," in *A Parametric Characteristic Approach*, Springer, 2015.

[11] C. Cheng, Z. Peng, W. Zhang, and G. Meng, "Volterra-series-based nonlinear system modeling and its engineering applications: A state-of-the-art review," *Mechanical Systems and Signal Processing*, vol. 87, pp. 340–364, 2017.

[12] J. Prawin and A. R. M. Rao, "Nonlinear identification of mdof systems using volterra series approximation," *Mechanical Systems and Signal Processing*, vol. 84, pp. 58–77, 2017.

[13] X. Jing, Z. Lang, and S. A. Billings, "Determination of the analytical parametric relationship for output spectrum of volterra systems based on its parametric characteristics," *Journal of mathematical analysis and applications*, vol. 351, no. 2, pp. 694–706, 2009.

[14] Q. Ran, M. L. Xiao, and Y. X. Hu, "Nonlinear vibration with volterra series method used in civil engineering: The bouc-wen hysteresis model of generalized frequency response," in *Applied Mechanics and Materials*, vol. 530, pp. 561–566, Trans Tech Publ, 2014.

[15] A. Maachou, R. Malti, P. Melchior, J.-L. Battaglia, A. Oustaloup, and B. Hay, "Nonlinear thermal system identification using fractional volterra series," *Control Engineering Practice*, vol. 29, pp. 50–60, 2014.

[16] S. Billings and K. Tsang, "Spectral analysis for non-linear systems, part i: Parametric non-linear spectral analysis," *Mechanical Systems and Signal Processing*, vol. 3, no. 4, pp. 319–339, 1989.

[17] X. J. Jing, Z. Q. Lang, and S. A. Billings, "Mapping from parametric characteristics to generalized frequency response functions of non-linear systems," *International Journal of Control*, vol. 81, no. 7, pp. 1071–1088, 2008.

[18] L. Li and S. Billings, "Estimation of generalized frequency response functions for quadratically and cubically nonlinear systems," *Journal of Sound and Vibration*, vol. 330, no. 3, pp. 461–470, 2011.

[19] S.-J. Cheng and J.-J. Liu, "Nonlinear modeling and identification of proton exchange membrane fuel cell (pemfc)," *International Journal of Hydrogen Energy*, vol. 40, no. 30, pp. 9452–9461, 2015.

[20] J. Schoukens, T. Dobrowiecki, and R. Pintelon, "Parametric and nonparametric identification of linear systems in the presence of nonlinear distortions-a frequency domain approach," *IEEE Transactions on Automatic Control*, vol. 43, no. 2, pp. 176–190, 1998.

[21] R. Pintelon and J. Schoukens, "Measurement and modelling of linear systems in the presence of non-linear distortions," *Mechanical systems and signal processing*, vol. 16, no. 5, pp. 785–801, 2002.

[22] R. Pintelon, G. Vandersteen, L. De Locht, Y. Rolain, and J. Schoukens, "Experimental characterization of operational amplifiers: a system identification approach-part i: theory and simulations," *IEEE Transactions on Instrumentation and Measurement*, vol. 53, no. 3, pp. 854–862, 2004.

[23] A. De Angelis, J. Schoukens, K. Godfrey, and P. Carbone, "Best linear approximation of wiener systems using multilevel signals: Theory and experiments," *IEEE Transactions on Instrumentation and Measurement*, vol. 67, no. 5, pp. 1246–1253, 2017.

[24] A. Pavlov, N. van de Wouw, and H. Nijmeijer, "Frequency response functions for nonlinear convergent systems," *IEEE Transactions on Automatic Control*, vol. 52, no. 6, pp. 1159–1165, 2007.

[25] W. E. Vander Velde, *Multiple-input describing functions and nonlinear system design*. McGraw-Hill, New York, 1968.

[26] J. Peyton Jones and S. Billings, "Describing functions, volterra series, and the analysis of non-linear systems in the frequency domain," *International Journal of Control*, vol. 53, no. 4, pp. 871–887, 1991.

[27] P. Nuij, O. Bosgra, and M. Steinbuch, "Higher-order sinusoidal input describing functions for the analysis of non-linear systems with harmonic responses," *Mechanical Systems and Signal Processing*, vol. 20, no. 8, pp. 1883–1904, 2006.

[28] P. Nuij, M. Steinbuch, and O. Bosgra, "Measuring the higher order sinusoidal input describing functions of a non-linear plant operating in feedback," *Control Engineering Practice*, vol. 16, no. 1, pp. 101–113, 2008.

[29] P. Nuij, M. Steinbuch, and O. Bosgra, "Experimental characterization of the stick/sliding transition in a precision mechanical system using the third order sinusoidal input describing function," *Mechatronics*, vol. 18, no. 2, pp. 100–110, 2008.

[30] D. Rijlaarsdam, B. van Loon, P. Nuij, and M. Steinbuch, "Nonlinearities in industrial motion stages-detection and classification," in *Proceedings of the 2010 American Control Conference*, pp. 6644–6649, IEEE, 2010.

[31] D. Rijlaarsdam, P. Nuij, J. Schoukens, and M. Steinbuch, "Spectral analysis of block structured nonlinear systems and higher order sinusoidal input describing functions," *Automatica*, vol. 47, no. 12, pp. 2684–2688, 2011.

[32] H. Olsson, K. J. Åström, C. C. De Wit, M. Gäfvert, and P. Lischinsky, "Friction models and friction compensation," *Eur. J. Control*, vol. 4, no. 3, pp. 176–195, 1998.

[33] D. Rijlaarsdam, P. Nuij, J. Schoukens, and M. Steinbuch, "Frequency domain based nonlinear feed forward control design for friction compensation," *Mechanical Systems and Signal Processing*, vol. 27, pp. 551–562, 2012.

[34] L. Ucun and J. Salášek, "Hosidf-based feedforward friction compensation in low-velocity motion control systems," *Mechatronics*, vol. 24, no. 2, pp. 118–127, 2014.

[35] T. Tjahjowidodo, F. Al-Bender, and H. Van Brussel, "Friction identification and compensation in a dc motor," *IFAC Proceedings Volumes*, vol. 38, no. 1, pp. 554–559, 2005.

[36] D. Brown, G. Carbon, and K. Ramsey, "Survey of excitation techniques applicable to the testing of automotive structures," tech. rep., SAE Technical Paper, 1977.

[37] J. Schoukens, R. Pintelon, and Y. Rolain, *Mastering system identification in 100 exercises*. John Wiley & Sons, 2012.

[38] P. Eykhoff, "System identification: parameter and state estimation," 1974.

[39] J. S. Bendat and A. G. Piersol, "Engineering applications of correlation and spectral analysis," *New York, Wiley-Interscience, 1980. 315 p.*, 1980.

[40] Z.-F. Fu and J. He, *Modal analysis*. Elsevier, 2001.

[41] Y. Liu, J. Li, Z. Zhang, X. Hu, and W. Zhang, "Experimental comparison of five friction models on the same test-bed of the micro stick-slip motion system," *Mechanical Sciences*, vol. 6, no. 1, pp. 15–28, 2015.

[42] J.-C. Shen, Q.-Z. Lu, C.-H. Wu, and W.-Y. Jywe, "Sliding-mode tracking control with dnlrx model-based friction compensation for the precision stage," *IEEE/ASME Transactions on Mechatronics*, vol. 19, no. 2, pp. 788–797, 2013.

[43] P. Cui, D. Zhang, S. Yang, and H. Li, "Friction compensation based on time-delay control and internal model control for a gimbal system in magnetically suspended cmg," *IEEE Transactions on Industrial Electronics*, vol. 64, no. 5, pp. 3798–3807, 2016.

[44] P. Eamcharoenying, A. Hillis, and J. Darling, "Friction compensation using coulomb friction model with zero velocity crossing estimator for a force controlled model in the loop suspension test rig," *Proceedings of the Institution of Mechanical Engineers, Part C: Journal of Mechanical Engineering Science*, vol. 230, no. 12, pp. 2028–2045, 2016.

[45] L. Lu, B. Yao, Q. Wang, and Z. Chen, "Adaptive robust control of linear motors with dynamic friction compensation using modified lugre model," *Automatica*, vol. 45, no. 12, pp. 2890–2896, 2009.

[46] J. Yao, W. Deng, and Z. Jiao, "Adaptive control of hydraulic actuators with lugre model-based friction compensation," *IEEE Transactions on Industrial Electronics*, vol. 62, no. 10, pp. 6469–6477, 2015.

[47] C. Li, Z. Chen, and B. Yao, "Identification and adaptive robust precision motion control of systems with nonlinear friction," *Nonlinear Dynamics*, vol. 95, no. 2, pp. 995–1007, 2019.

[48] E. Sincar, "Friction identification and compensation in stabilized platforms," Master's thesis, Dept. Mech. Eng., Middle East Technical University, Ankara, Turkey, 2013.